Aalto University
School of Chemical Technology
Degree Programme in Chemical Technology

Irene Coronado Martín

Carbon Dioxide Methanation for Intensified Reactors

Master's Thesis
Espoo, March 9, 2015

Supervisor: Professor Juha Lehtonen, Aalto University
Advisers: Professor Jukka Koskinen, Aalto University
Francisco de S. Vidal Vázquez M.Sc. (Tech.), VTT

Aalto University
School of Chemical Technology
Degree Programme in Chemical Technology

Abstract of
Master's Thesis

Author:	Irene Coronado Martín		
Title:	Carbon Dioxide Methanation for Intensified Reactors		
Supervisor:	Professor Juha Lehtonen		
Advisers:	Professor Jukka Koskinen Francisco de S. Vidal Vázquez M.Sc. (Tech.)		
Professorship:	Chemical Technology	**Code:**	Kem-40
Date:	March 9, 2015	**Pages:**	vii + 83
Language:	English		

The present work is related to the development of sustainable energy systems based on the Power-to-Gas concept. The main objective is to utilise renewable hydrogen and carbon dioxide to produce methane for storage in the natural gas infrastructure.

Multitubular fixed-bed reactors are established at industrial scale for CO_2 methanation. Catalytic pellets commonly loaded in this type of reactor involve poor heat transfer and high pressure drop that lead to inefficient processes. Today, reaction engineers focus their research on the branch of process intensification. Highlighted features of intensified reactors are improved heat and mass transfer, product efficiency, and reduced size.

VTT Technical Research Centre of Finland is developing a technology in reactor intensification which includes the development of novel catalyst deposition methods by washcoating and nanocoating. The aim of this work was to determine the suitability of these novel catalysts for CO_2 methanation, and the optimal operation conditions that favour their performance. Washcoated and nanocoated catalysts were tested in laboratory scale and compared with conventional packed-bed catalysts. The reactors were loaded with nickel-based catalysts and operated at three different temperatures (350, 400, and 500^{0}C) and three different flow rates (0.7, 1.0 and 1.3 ln/min), H_2:CO_2 = 4, and at atmospheric pressure.

The catalyst bulk density of washcoated reactors was significantly lower than in packed-bed reactors. As a result, the washcoated catalysts performed better due to more efficient heat transfer and temperature control. Carbon dioxide conversion equal to 69% and 99% methane selectivity were obtained with the washcoat with highest nickel content at 410^{0}C. The good results obtained with washcoated reactors encourage the development of these reactors into scaled-up configurations. Conversely, nanocoated catalysts exhibited lower performance. Nevertheless, the possibility of developing active catalysts minimizing the content of active phase motivates further research on the nanocoating technology.

Keywords: carbon dioxide, methanation, washcoating, nickel catalyst, intensified reactor, power-to-gas

Acknowledgements

This Master's thesis has been conducted in the team of Catalysis and Synfuels of VTT Technical Research Centre of Finland for the NEO-CARBON ENERGY project, between August 2014 and February 2015.

I am grateful for the feedback and comments from professors Juha Lehtonen and Jukka Koskinen, Francico de S. Vidal Vázquez, Pekka Simell, and Johana Kihlman. They all helped me to improve my thesis. I am also grateful to Mari-Leena Koskinen-Soivi and the personnel working in the lab for their assistance during the experimental part of this work.

Additionally, I thank Pekka Simell for giving me the opportunity of performing this Master's Thesis in VTT. The working environment and colleagues were really motivating and charming.

I also want to mention the support of my family and friends, especially those who are far away, but really close when I have needed them. "Todo esfuerzo tiene su recompensa".

Espoo, March 9, 2015

Irene Coronado Martín

Symbols and Abbreviations

GHSV	Gas Hourly Space Velocity (h^{-1})
$\dot{m}$	Mass flow rate (g/min)
m	Mass (g)
Mm	Molecular Mass (g/mol)
Q	Volume flow rate (ln/min)
S	Selectivity (%)
T	Temperature (^{0}C)
v	Concentration volume percentage (vol-%)
V_{Cat}	Volume of catalyst (m^3)
W_{Ni}HSV	Weight Hourly Space Velocity (h^{-1})
X	Conversion (%)
Y	Yield (%)

AC	Activated Carbon
CHP	Combinated Heat and Power
FID	Flame Ionization Detector
FT	Fishcer-Tropsch
GC	Gas Chromatograph
GTL	Gas To Liquid
HEX	Heat Exchanger
HY	Protonated Y zeolite
IGCC	Integrated Gasification Combined Cycle
IMRT	International Symposium on Microreaction Technology
MFEC	Microfibrous Entrapped Catalyst
MCM	Mobile Crystalline Material
MSM	Mesostructured Silica Nanoparticles
NG	Natural Gas
PEMFC	Proteon Exchange Membrane Fuel Cell
RHA	Rice Husk Ash
rWGS	Reverse Water Gas Shift

SNG	Synthetic or Substitute Natural Gas
TCD	Thermal Conductivity Detector
TPR	Temperature-Programmed Reduction

Contents

Chapter 1

Introduction

Reducing anthropogenic carbon dioxide emissions has been a major concern for many years. Carbon dioxide emissions have dramatically increased from a few thousands to tens of thousands of teragrams in the last hundred years. Today, 20% of the overall CO_2 emissions originate from energy generation [1]. Consequently, renewable sources have been the most popular alternative to the use of clean energy and reduction of carbon dioxide emissions.

In spite of the growing usage of energy from renewable sources, green fuels derived from these cannot compete against mature technologies of fossil fuels in terms of price. Therefore, parallel to green fuel development, another CO_2 control emission strategies, such as carbon dioxide capture and storage (CCS), have been the focus of much work in this field. This technology fights global warming by CO_2 collection and deep storage in the sea or in geological formations [2–6]. Capture and storage technology is taken a step further in the control of CO_2 emissions through carbon dioxide fixation. This approach suggests the utilization of CO_2 to produce chemicals, such as methanol [7], propylene carbonate [8], and Sn (II) complexes [9].

The need for renewable energy storage has generated much interest in the fixation of carbon dioxide through CO_2 methanation. In addition to carbon dioxide, a renewable hydrogen source should be considered for a sustainable Synthetic Natural Gas (SNG) production. Electrolytic hydrogen can be manufactured using energy surplus from fluctuating wind power and photovoltaic energy. As a result, captured CO_2 can be hydrogenated with renewable hydrogen to produce methane, storable in the already existing Natural Gas (NG) grid [10, 11]. The technology scheme involving the usage of renewable power to produce synthetic natural gas, the Power-to-Gas concept, is shown in Figure 1.1.

Producing chemicals or energy carriers from a renewable source of carbon offers a new market approach for the chemical industry while reducing atmo-

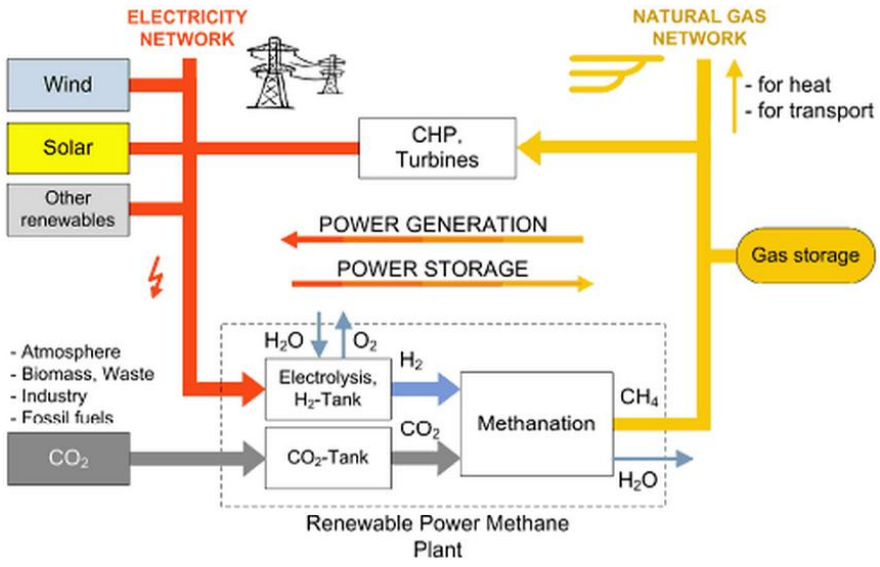

Figure 1.1: A renewable power-to-methane plant scheme (Wind/Solar-to-SNG) integrated into a power and gas grid [12].

spheric carbon dioxide concentration. However, the Power-to-Gas process could result in energy losses as high as 36%, as shown in Figure 1.2. Therefore, carbon dioxide methanation has been extensively studied to develop an efficient, economically feasible process for substitute natural gas production.

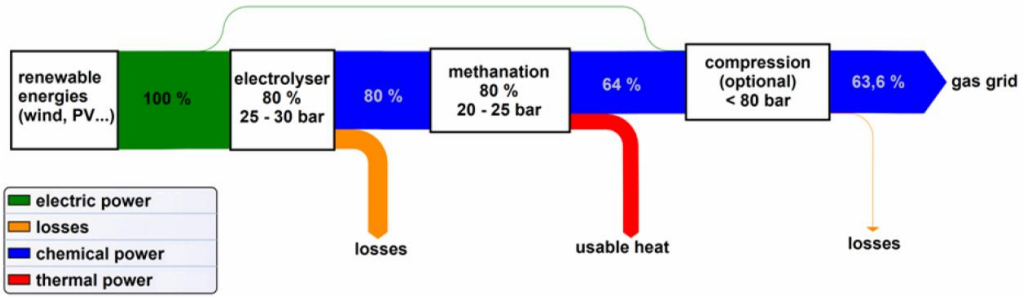

Figure 1.2: Sankey diagram for the synthesis of SNG based on renewable electricity [13].

Chapter 2

Objectives

Recently, much research has focused on finding a catalyst for CO_2 methanation with the best active metal-support combination [14–20]. These studies have provided significant information about the reaction kinetics and thermodynamic behaviours. However, little is yet known about the reaction mechanism of methanation. Furthermore, intensified reactors have been considered in order to improve methanation efficiency [21–26]. Process intensification has become a common practice since the 1990s. As a result, there is literature available on a large number of research works that test intensified reactors in reaction conditions within the scope of this work [27, 28]. However, not intensified reactor has been yet implemented for carbon dioxide methanation in industrial scale.

The aim of this thesis was to determine the suitability of novel catalysts for CO_2 methanation, and the optimal operation conditions that favour their performance. Pursuing this objective, novel catalysts developed in VTT Technical Research Centre of Finland were tested in laboratory scale.

Additionally, this thesis reviews the use of intensified reactors in general for highly exothermic and endothermic reactions, and specifically for carbon dioxide methanation. The main technologies for intensified reactors are assessed in order to determine the most convenient reactor technology at different reaction conditions. Furthermore, the thesis surveys the literature to analyse the principles of methane production, and common catalysts and reactors utilized in this reaction.

Chapter 3

Carbon Dioxide Methanation

Among the different technologies aimed at the reduction of atmospheric CO_2, Chapter 3 focuses on carbon dioxide fixation to produce synthetic natural gas. Carbon dioxide reduction through the Sabatier reaction was discovered in the 1910s. Nonetheless, it has recently renewed the interest of scientists in relation to the Power-to-Gas concept.

Composition of reactants for methanation and catalysts are subjects introduced in this chapter. Moreover, different reactors used in methanation and other exothermic reactions are reviewed as an introduction for the next Chapter 4 where intensified reactors will be more extensively analyzed.

3.1 Methane

Methane is the alkane with highest H/C ratio. This feature makes methane a high energy density hydrogen carrier. Hydrogen is the chemical element with highest mass energy density. However, this element has low mass, high flammability and high pressure requirements for its storage. These drawbacks complicate its production, transport, storage, and distribution for further use.

Natural gas grid is an infrastructure already available, which facilitates the storage and transportation of energy in form of methane [16]. Figure 3.1 shows energy storage technologies among which NG network has the largest capacity and the longest durability. Thus, methane has become a promising energy carrier of energy sources, such as the fluctuating solar energy and wind power.

Furthermore, the demand of NG have been affected by a significant rise in energy consumption [29]. Natural gas import in EU-27 virtually equals con-

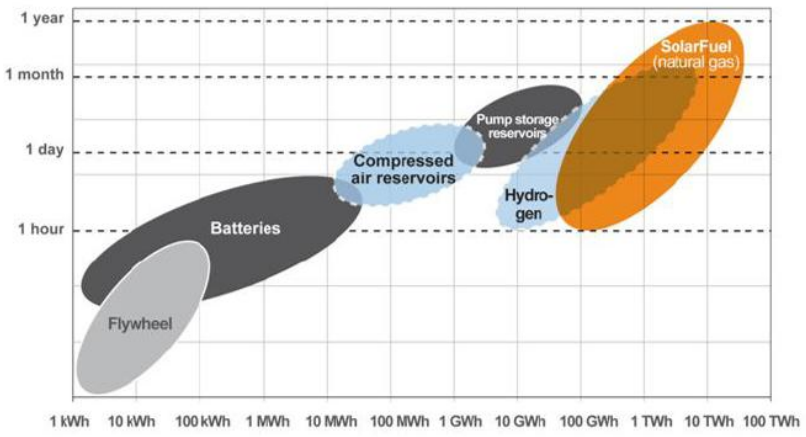

Figure 3.1: Electricity storage technologies in dependence on energetic storage capacity and charge cycling [11].

sumption (Figure 3.2). Therefore, synthetic natural gas production through methanation would constitute an economical asset to reduce gas import dependence.

Methane is a important component in the production of chemicals, such as ammonia, ethanol, dimethyl ether and hydrogen. Furthermore, liquid fuels can be produced from methane by means of fuel to liquid (FTL) technology through the Fischer-Tropsch (FT) reaction [30]. Additionally, the use of synthesis natural gas is promoted to detriment of fossil derived gas in Combined Heat and Power (CHP) plants [31].

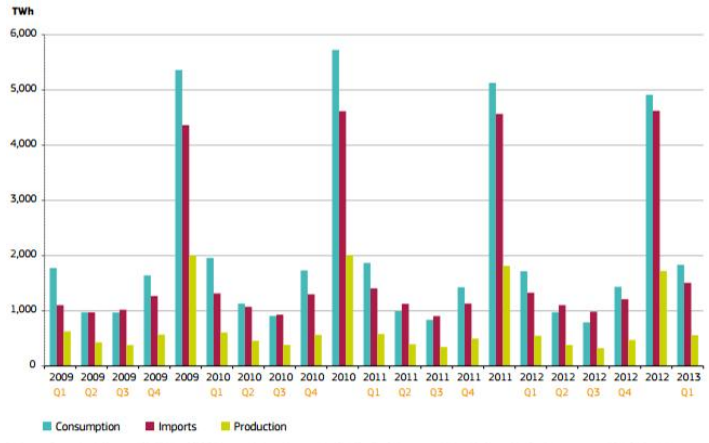

Figure 3.2: EU 27 gas consumption, imports and production [32].

3.2 Methanation

Synthetic natural gas is the target product of methanation (Equation 3.2). The reactants involved in this reaction are carbon dioxide and hydrogen which can be obtained from renewable sources leading to a sustainable production of methane.

Exhaust gases from power plants and simulated CO_2-rich gas mixtures have been utilized as a reactant for methanation [33]. Capture and utilization of CO_2 present in the exhaust gases of CHP plants and different production plants is a technology applicable to control CO_2 emissions [21].

In addition, methanation is widely used at hydrogen plants of oil refineries to remove CO from H_2-rich streams (Equation 3.1). Carbon monoxide methanation improves the quality of fuel cells inlet streams avoiding CO contamination of the membranes usually applied in proton exchange membrane fuel cells (PEMFC)[15].

$$CO + 3\,H_2 \longleftrightarrow CH_4 + H_2O \qquad \Delta H_R = -206,2 \quad kJ/mol \tag{3.1}$$

Regarding carbon dioxide methanation, there are different routes to produce synthetic natural gas. On the one hand, the Power-to-Gas thermochemical technology utilizes CO_2 derived from either the use of fossil sources or biomass gasification. On the other hand, the Power-to-BioGas technology, proposes the utilization of biological CO_2 originated in biogas plants [34].

$$CO_2 + 4\,H_2 \longleftrightarrow CH_4 + 2\,H_2O \qquad \Delta H_{278K} = -165,1 \quad kJ/mol \tag{3.2}$$

$$CO_2 + H_2 \longleftrightarrow CO + H_2O \qquad \Delta H_{298K} = 41,1 \quad kJ/mol \tag{3.3}$$

Both technologies involve carbon dioxide methanation, also called Sabatier reaction, in which the thermochemical methatantion of CO_2 occurs with hydrogen to produce methane and H_2O. Two different reaction mechanisms are usually proposed. According to the first mechanism, methanation occurs through CO_2 direct hydrogenation (Equation 3.2). The second mechanism propose the formation of intermediate carbon monoxide and subsequent CO methanation [35, 36]. This second mechanism is the most widely accepted, however, there is little information available [14]. A example of carbon dioxide methanation according to the second mechanism is shown in Figure 3.3.

Carbon dioxide methanation (Equation 3.2) is an equilibrium exothermic reaction with volume decrease. Hence, and according with the Le Chatelier's

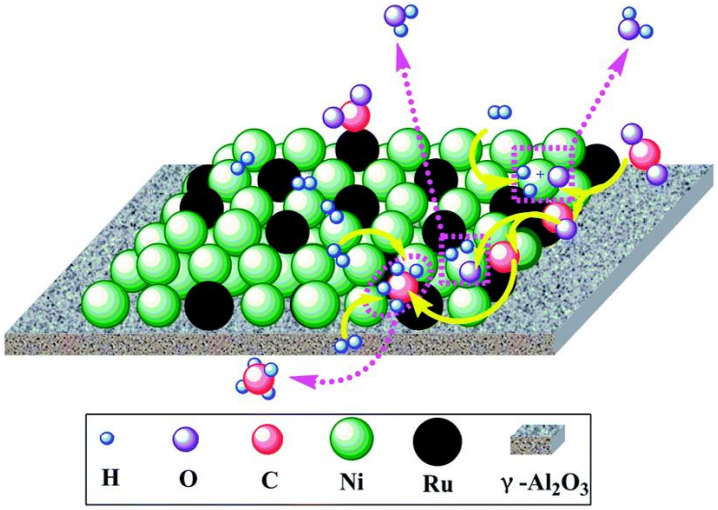

Figure 3.3: Proposed mechanism of CO_2 methanation over 10Ni-1.0Ru catalyst [37].

principle, to promote methane production, Sabatier reaction should be performed at low temperature and high pressure. In relation with the previous statement, achieving high methane yields with fine selectivity is possible if the reaction is carried out at low temperature. Elevated temperature, on the one hand, shifts the equilibrium towards the reactants, diminishing CO_2 conversion. And on the other hand, promotes the endothermic reverse water gas shift (rWGS) reaction (Equation 3.3) [38], which reduces CH_4 selectivity in favour of carbon monoxide [17].

The statements made in the previous paragraph are proved in Figure 3.4 which shows the methanation equilibrium composition at different temperatures. The equilibrium composition at atmospheric pressure shows that CO_2 conversion and CH_4 selectivity reach the best values at low temperature (below 350 ^{0}C). Moreover, at temperatures above 500 ^{0}C, the CO selectivity increases in detriment of CH_4 selectivity and yield (Figure 3.4 and Figure 3.5 (b and c)). In addition, high pressure improves reactants conversion (Figure 3.5 (a)) and CH_4 yield.

In accordance with the chemical equilibrium composition, mild temperature is required in order to achieve good conversion. However, at low temperature, the reaction rate is lower [15]. As a consequent of the conflict between thermodynamic and kinetic limitations a good temperature control and an active catalyst are requested for the efficient production of SNG.

Other parameter affecting methanation performance is the H_2/CO_2 ratio which has been studied by Rahmani *et al.* [17]. This work proved that ratios above the stoichiometric (from 4 to 7) improve conversion values, and reduce carbon deposition [36]. This probably happens as a consequence of changes in the reaction mechanism [15]. Figure 3.6 shows that H_2/CO_2 ratio

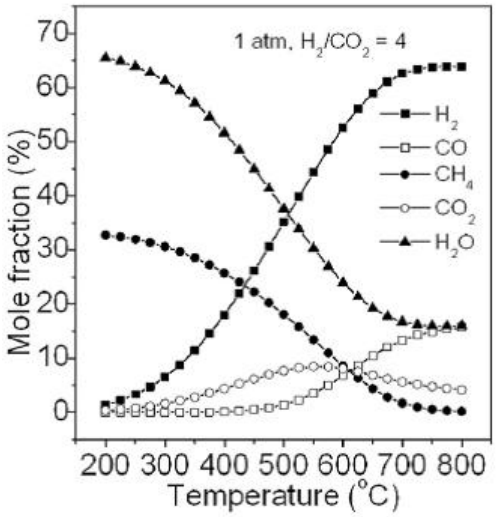

Figure 3.4: Product fraction of CO2 methanation at equilibrium [36].

equal or above the stoichiometric leads to high conversion, selectivity and yield. However, within the range of temperature where CO_2 methanation is favoured (350-400 ^{0}C) the methanation performance improvement due to higher ratio of the reactants is minor.

In summary, Sabatier reaction is an exothermic volume descendent reaction. Hence, CO_2 conversion, and CH_4 selectivity and yield are enhanced at low temperatures, elevated pressure, and at or above stoichiometric ratio of the reactants. Temperatures between 300 and 450 ^{0}C, atmospheric pressure, and reactants stoichiometric ratios are conditions often presented in publications of research studies performed in laboratory scale (Table 3.2) [35, 39].

3.3 Feedstock

Carbon dioxide and hydrogen are the reactants taking part in CO_2 methanation. There is a large number of fossil CO_2 sources, such as power and chemicals plants [40]. However, integration with bioenergy plants are preferred in order to promote entirely renewable technologies [12]. In section 3.2, CO_2 sources, such as biomass and biogas plants, were mentioned in regard with the Power-to-gas and the Power-to-BioGas technologies. Moreover, these technologies consider hydrolysis of water as a feasible and sustainable hydrogen source.

The reactants are normally accompanied by impurities which vary depend-

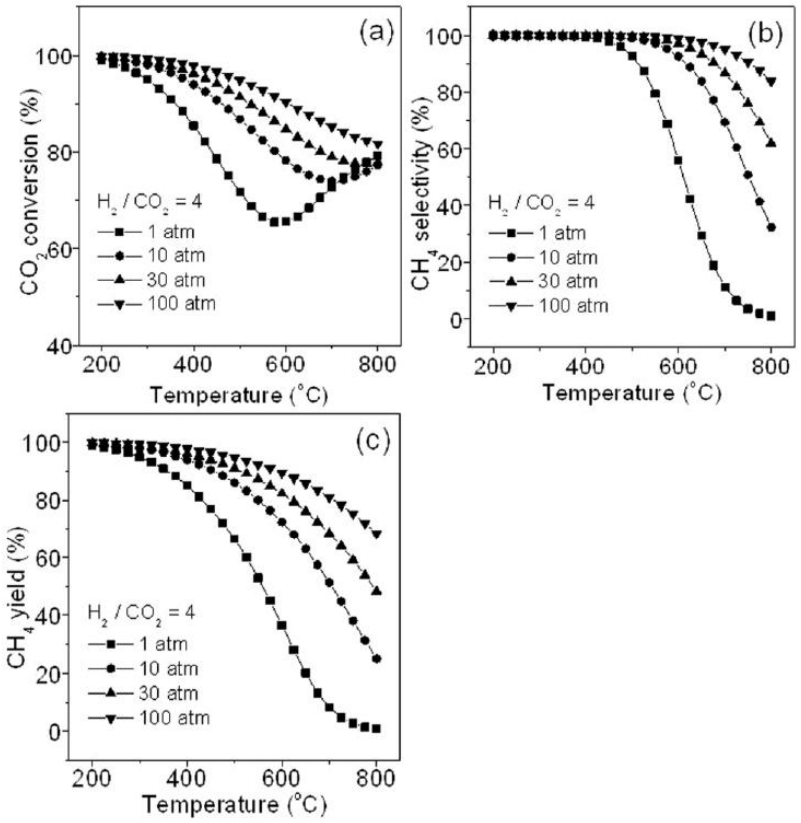

Figure 3.5: Effects of pressure and temperature on CO_2 methanation: (a) CO_2 conversion, (b) CH_4 selectivity, (c) CH_4 yield [36].

ing on the source. Hydrolytic hydrogen is only accompanied by oxygen, however, carbon dioxide might be part of gas mixtures with diverse compositions. Some of the components in the CO_2-rich streams might cause poisoning of the active sites of the catalyst causing severe changes in the catalytic activity. This section will review different sources of carbon dioxide in order to know the possible contaminants present in methanation inlet stream and their effect on the reaction parameters.

In power plants, exhaust gases derived from combustion processes include SO_x, NO_x, O_2 and N_2. Other components, such as argon, nitrogen and oxygen, may be found when the gases are derived from pure oxygen combustion, also called oxyfuel process. On the other hand, in exhaust gases derived from gasification process, or integrated gasification combined cycle (IGCC), where also combustion takes place, regular contaminants are H_2S and CO. Additionally, H_2O appears along with the previously mentioned components, independently of the feedstock used in the plant [12, 41].

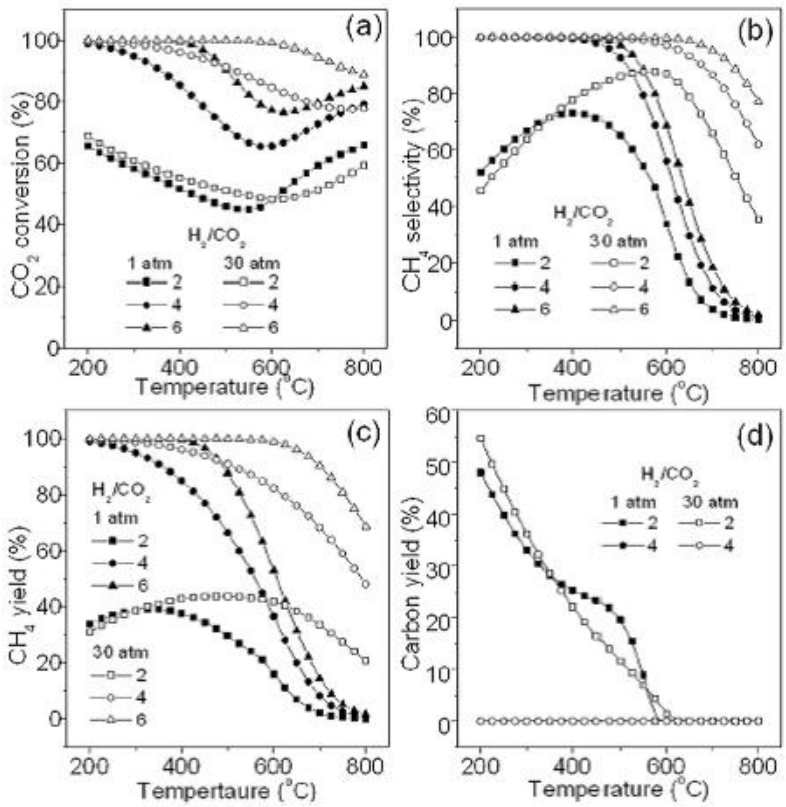

Figure 3.6: Effect of H_2/H_2 ratio on CO_2 methanation: (a) CO_2 conversion, (b) CH_4 selectivity, (c) CH_4 yield, and (d) carbon yield [36].

Nitrogen and oxygen are components often present in industrial exhaust gases. Regarding the concentration of N_2, it should be minimized to reduce downstream separation costs. Furthermore, the presence of O_2 affects the catalytic activity and by-products formation, and thus, its concentration must be controlled. Table 3.1 shows recommended concentration ranges of methanation inlet mixture gases and in CO_2-rich stream to avoid catalyst poisoning [40].

An experimental study was performed in a packed bed reactor where nickel catalyst supported on silica gel was tested for methanation using power plant exhaust gases. The study shows how conversion, yield, and selectivity are affected by the presence of SO_2 and NO_2, or oxygen in the inlet gas. While nitrogen dioxide does not practically influence the reaction, sulphur dioxide cause decrease of CO_2 conversion due to catalyst deactivation. Nevertheless, in this study it was claimed that the presence of H_2S in the feedstock would cause more noticeable activity loses than SO_2 does. In

Component	Unit	Value for methanation input	Value for CO_2 stream
H_2	Vol.%	35–80	–
CO_2	Vol.%	0–30	0–100
CO	Vol.%	0–25	0–100
CH_4	Vol.%	0–10	0–50
N_2	Vol.%	<3	<15
O_2	Vol.%	n.s.	n.s.
H_2O	Vol.%	0–10	0–50
Particles	mg/scbm	<0.5	<2.5
Tar	mg/scbm	<0.1	<0.5
Na, K	mg/scbm	<1	<5
NH_3, HCN	mg/scbm	<0.8	<4
H_2S	mg/scbm	<0.4	<2
NO_x	mg/scbm	n.s.	n.s.
SO_x	mg/scbm	n.s.	n.s.
Halogens	mg/scbm	<0.06	<0.3

n.s.: not specified, *scbm:* standard cubicmeter (20 °C, 0.1 MPa)

Table 3.1: Gas quality for methanation [40].

cases where O_2 accompanied CO_2 in the feedstock, selectivity was not significantly disturbed. However, yield and conversion were lower due to the undesired reaction of hydrogen with oxygen [33].

3.4 Catalysts

Methanation requires the presence of an active catalyst in the reaction medium to increase the reaction rate at relatively low operation temperature. The use of different active metal-support combinations have been studied in several publications to achieve good levels of activity and selectivity under different reaction conditions [39]. Some representative results are presented in Table 3.2.

Generally, metals belonging to the group VIII, such as Ni [17], Ru [45], Rh [19], and Cu [18], provide good reaction rate for methanation. These metals are often supported on oxides to enhance their dispersion and stability. Some highlighted support materials are mesostructured silica nanopaticles (MSN), Mobile crystalline material (MCM), (protonated Y zeolite) HY, SiO_2,and γ- Al_2O_3 [15]; CeO_2 and Al_2O_3 [16]; TiO_2 [22]; and nickel β-zeolite [46].

Catalyst	t stream (h)	T (^{0}C)	GHSV	X_{CO2} (%)	S_{CH4}	Ref.
$LaNiO_3$ [a]	N/A	300	7 500 h^{-1} [b]	77.7	99.4	[39]
Ni/MSN	N/A	300	50 000 h^{-1} [b]	64.1	99.9	[15]
15Ni-$Ce_{0.72}Zr_{0.28}O_2$	150	350	43 000 h^{-1}	75.9	99.1	[42]
5Ni-C/Z(60-40)	150	350	43 000 h^{-1}	65.9	98.2	[43]
Ni/La_2O_3	2	350	30 000 h^{-1}	97.7	100	[44]
20Ni/Al_2O_3 [c]	1	350	9 000 h^{-1} [b]	71	99	[17]
Pd-Mg/SiO_2	3,06 $\times 10^{-4}$	450	N/A	59.2	95.3	[35]

Table 3.2: Comparison of catalysts activity for CO_2 methanation at 1 atm and H_2/CO_2=4.

[a] Reaction pressure = 15 atm
[b] Unit change δ_{cat} = 1 g/cm^3
[c] Reactants ratio H_2/CO_2 = 3.5

Wang *et al.* [14] performed an extensive methanation study where different solid catalysts were assessed. Their work focused on the most widely used nickel-based catalyst, to compare these with other metal-based catalysts. The most significant conclusion is the importance of achieving a stable metal-support interaction. In addition, the comparative study of Aziz *et al.* [15] of different nickel supported catalysts demonstrated little or no deactivation and satisfactory catalytic activity in long-term stability test. Ultimately, nickel based are considered the most suitable methanation catalysts due to their high activity, selectivity, and moderate cost [17].

Furthermore, improved catalyst combinations have been developed regarding the different steps in the reaction mechanism of methanation. Combining Rh/γ-Al_2O_3 and Ni/AC (nickel-activated carbon) has been proved to have a positive effect on carbon dioxide reduction. The former catalyst promotes the kinetically limited carbon dioxide adsorption and dissociation steps, while Ni/AC catalyst induces similar effect for H_2 molecules [19].

Apart from the aforementioned catalysts, perovskites are noteworthy catalysts in development stage. These materials are characterized by high catalytic activity and stability which allow elevated operating temperatures. Additionally, perovskite catalyst enable high dispersion within components with molecular formulas ABO_3, presented in 3.7 (e.g. $CaTiO_3$), $AB_{1-x}B_xO_3$ (e.g. $TiCa_{1-x}Sr_xO_3$), A_2BO_4 (e.g. C_2BaO_4) [39]. Figure 3.7 shows common substituents which are metals with larger radius in the A site, and metals from transition group, with smaller radius in the B site [47]. Section 4.3 provides more detailed information about perovskites materials, and experimental studies where these components have been applied to reactive systems.

In summary, the selection of different active metal-support combinations is a crucial decision that will set the reaction conversion, selectivity, yield, and

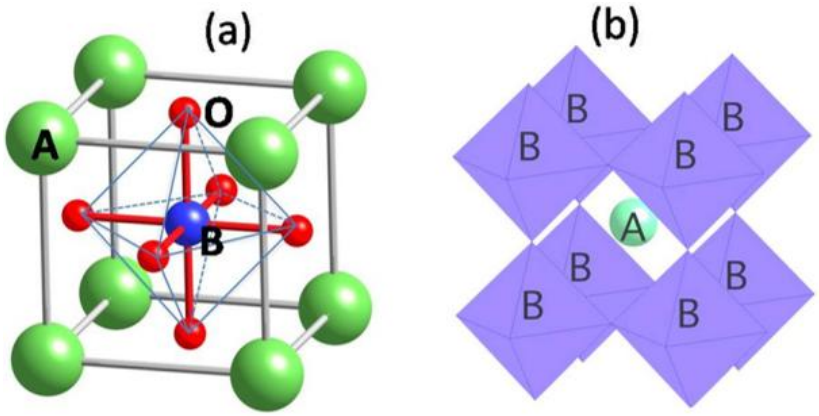

Figure 3.7: The structure of an ABO_3 perovskite with the origin centred at (a) the B-site ion and (b) the A-site ion [48].

stability levels in methanation. Thus, catalyst supports used in methanation should provide a right dispersion of catalyst active sites maintaining high reaction rate at demanding conditions.

3.5 Reactors

Carbon dioxide in a strongly exothermic reaction which requiring good temperature control. Therefore, the main factor to consider in the reactor design of this reaction is the heat removal capacity. Thus, in order to avoid significant temperature gradients and hot spot formation, reactor must provide good heat exchange rate. The state-of-the-art of methanation reactors, including packed bed reactor and other alternatives, is reviewed in this section.

Packed bed with pellets are established and well known reactors, easy and inexpensive to construct and operate, utilized in a large number of reactions. These type of reactors constitute a cylinder filled up with pellets where the catalyst is deposited [49]. In spite of being a widely used reactor, packed beds have drawbacks influencing negatively some of the reaction parameters. These reactors have low efficiency in energy consumption due to high values of pressure drop [50]. In addition, isolated contact points among pellets derives in a poor heat transfer. Increasing the flow rate or reducing the size of pellets are ways of improving the heat and mass transfer. However, these measures also increase the pressure drop [51]. Therefore, a compromise with particle size should be made for a suitable pressure drop, and heat and mass transfer.

Several enhancements aimed at heat exchange improvement are introduced in the conventional packed bed reactors with industrial application to avoid hot spots formation and temperature runaway. Adiabatic packed-bed reactors in series with intermediate cooling systems and gas recycling is an example of reactors employed for methanation [31]. However, this highly exothermic reaction demands more efficient equipment in terms of heat evacuation, such as multitubular reactors. The inner structure of non-adiabatic multitubular reactors consist of up to thousands tubes packed with the catalyst and externally cooled down [49]. An industrial example of methane production in multitubular reactor is represented by the Power-to-gas plant of Etogas [52]. Comparing adiabatic and isothermal processes, the latter entails mild operating conditions, and generates high-pressure steam, which make them more energetically efficient [53].

A different reaction concept, such as fluidized bed reactors, is usually considered to improve heat exchange and operate at close to isothermal conditions. However, unsteady operation and catalyst abrasion problems in fluidized bed reactors make infeasible the scale-up to methanation industrial plants. Slurry reactors are a second non-adiabatic option for SNG production. In this 3-phase reactors, catalyst particles and the reactants are mixed with a heat transfer liquid which allows near isothermal operation [40]. Bajohr and Götz [13, 54] have extensively studied CO_2 methanation performed in 3-phases bubble column reactors, and compared with other conventional systems. Slurry columns present clear advantages compared with packed bed reactors. However, drawbacks such as mass transfer restrictions and selection of the heat transfer liquid should be overcome for future commercial applications.

Process intensification has been the focus of much work seeking a promising alternative to develop novel non-adiabatic systems [53]. Intensified reactors bring intrinsic features, such as size reduction, enhanced transport properties, and low-energy consumption, which are necessary for the implementation of more efficient technologies [49].

Several research works have confirmed improvements in the performance of intensified reactors in contrast to packed bed reactors. Schlereth *et al.* [25] compared packed bed and membrane fixed bed reactors for CO_2 methanation. There was a clear enhancement regarding to mass and hear transfer, and reaction rate. This fact is a direct consequence of a better temperature control, facilitated by controlling the reactants supply through a membrane. Furthermore, according to the research conducted by Yoshida *et al.* [21], honeycomb monoliths fixed reactors enable superior reaction rate and conversion in carbon monoxide methanation compared to conventional packed bed reactors.

Commercial reactors used in gas-solid systems, as methanation, present limitations in terms of heat and mass transfer, and pressure drop. Therefore, Chapter 4 will focus on the description and assessment of intensified reactors which have appropriate features for highly demanding reaction conditions in terms of transport phenomena.

Chapter 4

Intensified Reactors

Process intensification has been a developing trend in the chemical engineering sector for the last 30 years. Intensified technologies enables considerable enhancements in the equipment conventionally used in unit processes of the chemical industry. Some of the most relevant objectives of process intensification are to achieve energy and production efficiency increase, lower operation costs, environmentally friendly and safer processes, and plant size reduction [55].

Common features characterizing intensified reactors are improved control of temperature and reduction of hot spot formation, shorter residence times, and thus, enhanced production efficiency. Furthermore, reduction of mass transfer limitations lead to increased productivity. Additionally, reactor size reduction and lower catalyst loading decrease investment costs.

Intensified reactors may overcome significant drawbacks of traditional reactors. Thus, growing relevance of process intensification and the inherent drawbacks of traditional reactors, have launched a new generation of reactors presented in this chapter. Today, reaction engineers focus their research on the branch of process intensification. Chapter 4 reviews common types of intensified reactors targeted to heterogeneously catalysed reactions with demanding operation conditions.

4.1 Microchannel Reactors

Microreactors are constructions designed in microns scale [56]. Microchannel reactors consist of metallic sheets with etched microchannels (Figure 4.1) where the catalyst is deposited [49]. This type of reactors have intensified heat transport properties. Therefore, they have gained importance specially

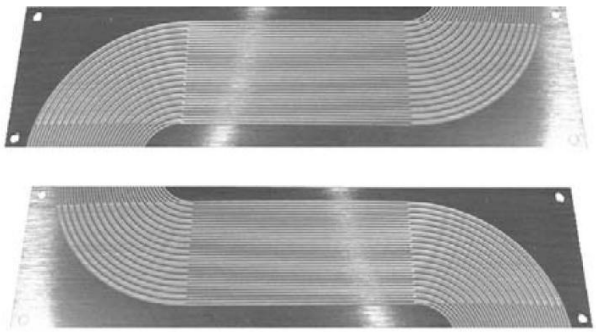

Figure 4.1: Microstructured plates for microreactor [58].

for highly endothermic or exothermic reactions which require a proper heat management.

Microchannel reactors are a new technology far from the traditional reactor concepts. Therefore, research regarding this type of reactors must be done before the fully implementation in industrial scale [51]. An example of the effort invested in this technology is The International Symposium on Microreaction Technology (IMRET) which has organized conferences since 1995 for the purpose of reviewing the advances in microreactor technology [57].

The amount of publications in the area of microreactors is extensive. Kolb *et al.* [27] reviewed many research works regarding the use of microstructured reactors in heterogeneously catalysed systems. Foremost conclusion of this review is the importance of temperature control over conversion, selectivity, yield, or residence time, and how they are usually improved in microstructured configuration in contrast to conventional packed-bed reactors.

Compactness is one of the main features of microchannel reactors with considerable low reaction-volume-to-surface-area ratio. As a consequence,these reactors reach heat transfer rates comparable to those of heat exchangers [50]. Furthermore, microreactors compactness [23] allows thinking of hydrogen production intended for mobile and small transportation systems [59]. In addition, miniaturized reactors would reduce investment and operating costs of pilot plants, simplifying the step from lab to pilot scale [60].

Thermodynamically demanding steam reforming and partial oxidation comprise highly endothermic and exothermic reactions for H_2 production. Heat management in reformers has been a problem in terms of cold and hot spots development because of temperature control difficulties. Accordingly,

various studies have been addressed to create a synergy system between exothermic and endothermic reactions. For instance, Zanfir *et al.* [61] simulated a procedure where methane combustion provided heat to endothermic methane steam reforming in a coated-plate reactor. Common temperature gradients in conventional reformers were diminished by 200 K when using a microchannel reactor.

Tonkovich *et al.* [62] applied similar procedure for the coupled steam reforming and partial oxidation of methane. The Velocys microchannel reformer used in this work consists of a series of Inconel plates washcoated with catalyst in the reforming side of the reactor. The catalyst involved in the partial oxidation was inserted in the reactor channels in the form of a metallic foam. The reaction in the microchannel system showed excellent temperature control, decrease of mechanical demands, and reduction in NO_x emissions. The American company Velocys [63] has developed intensificated systems applied to highly exothermic and endothermic gas to liquid technologies. The microreactors that Velocys commercialize are characterized by efficient and environmentally friendly equipment. This is possible due to enhanced heat and mass transfer, and straight forward number-up [62].

Increasing pressure, feed concentrations, or temperature until runaway or explosive regimes, are different ways to intensify reaction conditions. In microstructured reactors, process intensification may be applied within safety limits in order to increase reaction rates [27, 56, 64]. Lange *et al.* [64] experimented with partial oxidation of o-xylene in a microchannel reactor filled up with pellets of V_2O_5/TiO_2 forming a packed-bed. The reactor was operated within the explosion limits, which is not usually possible for conventional reactors. Moreover, these operation conditions enabled a feed above stoichiometry composition maintaining still the normal range of selectivity.

Foremost advantages in the use of microstructured reactors are the intrinsic features of process intensification, including wider operation regimen, excellent heat management, and lower residence time. However, there are drawbacks such as economies of scale, due to the ratio of construction material to reactor volume, and mass transfer, limited by laminar flows. In other words, diffusion is the only possible transport mechanism in laminar flow. A possible enhancement of diffusion is by narrowing the reactor channels [56].

Moreover, low catalyst loading is also a hindrance against the development of this technology due to low bulk density of catalyst. The high surface-to-volume ratio that provide excellent heat transport features, becomes insufficient in terms of catalyst loading. While packed beds usually have contact area about 10^8 m^2/m^3, microreactors reach only near $2x10^4$ [65].

On the one hand, packed-bed have are industrially well known catalysts. However, high pressure drop and limited heat transport promote searching alternative methods for catalyst loading. On the other hand, coatings deposited in the reactor wall enables non-adiabatic conditions and uniform temperature distributions [58, 65]. Nonetheless, catalytic walls usually offer insufficient contact surface area between catalyst and reactants. Therefore, different coating methods, such as washcoating, sol-gel technology, slurry coating, chemical vapor deposition, and flame combustion synthesis are being developed to improve the catalytic activity [58].

4.1.1 Micropacked-bed Reactors

Catalytic pellets constitute the fixed-bed of microchannel reactors similar to the one shown in Figure 4.2. The main advantages of packed beds are high surface contact area, and easy catalyst loading. Knochen *et al.* [66] considered packed beds as a feasible option for catalyst implementation in microchannel reactors. This conclusion was based on a simulated Fischer-Tropsch reactor which showed acceptable pressure drop at high conversions, and volume decrease.

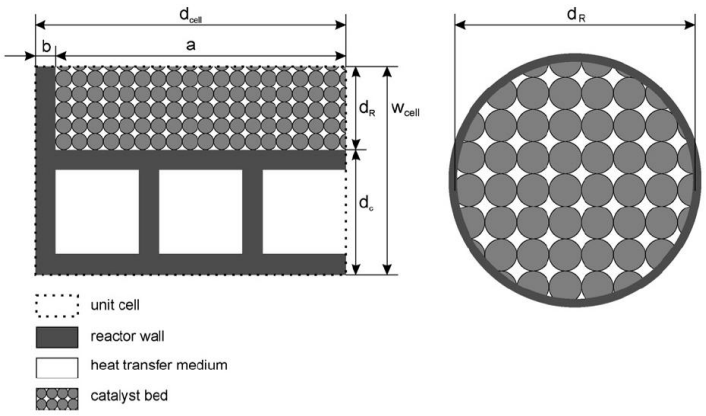

Figure 4.2: Reactor configurations for microstructured fixed-bed reactors [66].

The size of the pellets utilized in microstructured packed-bed reactors is the main hindrance of industrial applications due to high pressure drops [64]. Alternatively, wall-coating is proposed for several authors in order to combat that drawback and improve heat transfer.

4.1.2 Wall-coated Reactors

Coating consist of depositing catalytic material as a thin layer on the microchannel surface. Important considerations concerning coating processes are mechanical stress, interaction and chemical compatibility, and active metal dispersion [65]. Furthermore, channel height and catalyst-coat thickness have demonstrated to have huge influence in the conversion and temperature. Thicker catalyst layer may lead to diffusion limitations in the catalyst layer [61].

Improved efficiency was demonstrated in the selective CO_x methanation conducted in a microchannel-plate reactor coated with Ru/SiO_2 and Ru/Al_2O_3. The experimental results showed high conversion (95%) at nearly constant low temperature (about 300 ^{0}C) [67]. Accurate temperature control makes this type of reactor appropriate for experimental studies and kinetic data extraction [23, 67]. In a later work, Gorke *et al.* were able to reduce yields of side products in ethanol reforming. The reactor consisted of etched foils with 200 μm wide and 200 μm deep channels coated with Rh/CeO_2 catalyst. In this system the residence times were reduced which diminished by-products yield [59].

For the purpose of testing catalytic activity and reaction efficiency, Men *et al.* [23] carried out methanation in a microchannel reactor. The etched plates reactor, with 500 μm wide and 250 μm deep channels, were washcoated with a 20 μm thick layer. Ruthenium and nickel-based catalyst on CaO/Al_2O_3 support were applied. As a result, a strong correlation was found between conversion and the amount of active metal loaded on the microchanneled plates. Similar study was performed for CO methanation by Galletti *et al.* [45]. These authors obtained enhanced activity with lower load of active metal and thicker coatings in the microchannel reactor coated with Ru/γ-Al_2O_3.

Coated channels enhance reaction rate and temperature control in the reactors. Consequently, temperature gradients are minimized resulting in lower catalyst deactivation rate, lengthening the catalyst life [65]. However, low catalyst loading as well as catalyst loading and unloading in regeneration cycles still constitutes a technical problem.

4.2 Structured Reactors

Metallic or ceramic fixed arrangements coated with a thin layer of catalytic material constitute the inner framework of structured reactors (Figure 4.3). This structured configurations facilitates fluid mixing, and shorter residence

time and pressure drop. These features can overcome some common barriers present in fixed-bed reactors [50].

Noteworthy improvements of structured reactors in comparison with packed beds are lower pressure drop and, enhanced heat and mass transfer. High heat transfer rates of metallic material optimizes product selectivity due to reduction of secondary reactions. On the other hand, high mass transfer is an advantage also compared with microchannel reactors. These characteristics will result in more compact reactors with lower investment costs in upscaled equipment [51].

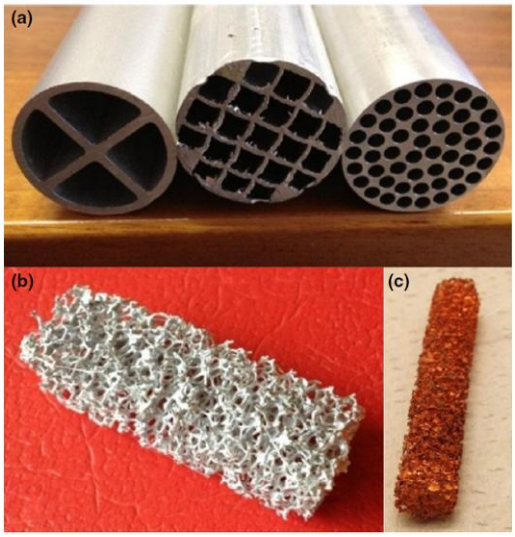

Figure 4.3: Conductive structured substrates for adiabatic applications: (a) aluminum honeycomb monoliths, (b) aluminium open-cell foam, (c) copper open-cell foam [51].

4.2.1 Honeycomb monoliths

Monolith reactors have found the most extensive application in the automotive sector as catalytic converters [49].Furthermore, features such as heat transfer ability in metallic monoliths makes these structures attractive for thermally demanding reactions.

Materials commonly used in monolith manufacture are porous ceramics and metals. Usual cross sectional shape is triangular, square or hexagonal, coated with catalyst (Figure 4.3 (a)). Mathematical models showed improved heat transfer over triangular and square designs covered with catalytic having high thermal conductivity [68].

A bench scale test was performed for carbon dioxide methanation at a Japanese LNG power plant [21]. The reaction was carried out in a structured reactor with two different configurations. The reactor was packed with either catalytic pellets or honeycomb monoliths coated with nickel ferrite catalyst. The reaction rate was increased in the honeycomb system due to more efficient breakdown of CO_2 molecules. In addition, the scale-up of honeycomb monoliths to pilot size entailed reduction of the required amount of catalyst. About 10% of the quantity that would have been needed in packed-bed reactor was enough to achieve the desired conversion level in honeycombs. This was possible due to higher contact surface area in monoliths than in pellets fixed-bed, which improved mass transfer and catalyst availability.

4.2.2 Open-cell foams

Open-cell foams are ceramic or metallic highly porous structures (Figure 4.3 (b) and (c)). They are considered as static mixing packings with wide surface area, and mass and heat transfer abilities [49]. The main characteristics of open-cell foams are continuity and porosity which result in mass and heat transport enhancement [69].

Metallic open-cell foams are used as catalyst supports with low pressure drop [70], and as fillers with improved transport phenomena compared to packed-bed catalysts [51]. Simulations performed in order to study foam transport properties, showed pressure drop reduction in more porous configurations [71]. Furthermore, the typical adiabatic use of ceramic foams, improve radial heat transfer using metallic arrangements. For instance, structured foams such as FeCrAlY or Al-allow allow near isothermal conditions in exothermic and endothermic reactions [72]. Additionally, materials as SiC are suggested as construction materials of open-cell foams due to low cost and facilitated catalyst-loading cycles [73].

There is an obvious improvement of cell foams with regard to honeycomb monoliths. Uniform distribution of the components participating in the reaction in the axial and radial directions favours regular mass and heat transfer in the reactor [51]. However, the catalyst weight per reactor volume represent still a barrier against further development of open-cell foams [73].

4.2.3 Micro-fibrous Materials

Micro-fibrous reactors contain a metal, glass or polymeric inner structure [74] either covered or entrapped with catalyst particles [49] (Figure 4.4). The

clear advantage in terms of pressure drop, and mass and heat transport of structured over packed-bed reactors was presented in section Section 4.2. In addition, catalytic components deposited in the inner framework of metallic micro-fibrous materials provide higher active-surface area than in the other structured arrangements [51].

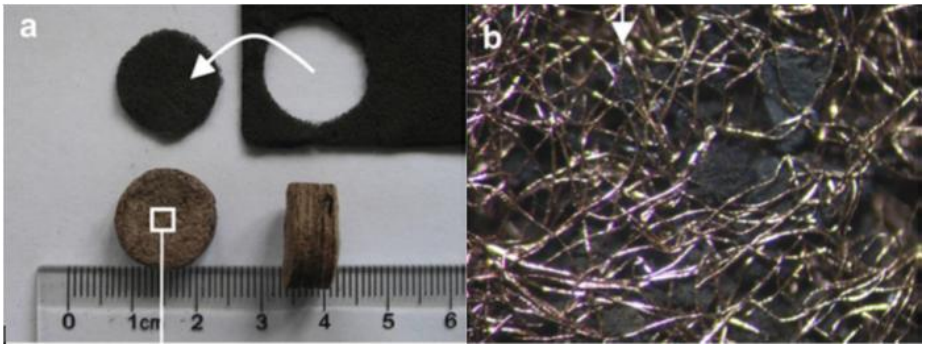

Figure 4.4: Macro- and micro-structure of Cu-MFE-Ni/AlO. (a) fresh (upper) and used (down) samples. (b) Optical photograph of used samples [75].

Continuous fibrous structure with high thermal conductivity allows proper heat management. Moreover, high availability of catalytic particles and large void volume result in efficient mass transfer and reduced pressure drop. Structures with significant voidage percentage offer considerable volume of entrapped catalyst with high stability and activity [76].

Chen *et al.* [75] studied endothermic dry reforming of methane over a microfibrous-nickel-based catalyst. The features listed in the previous paragraph led to enhanced conversion and temperature control in the microfibrous reactor compared with packed-bed reactor. Furthermore, surface-to-area-ratio was found five times higher in MFEC compared with microchannel and honeycomb monoliths. Additionally, according to Sheng *et al.* [77] temperature gradients decreased from 460 ^{0}C to 6.4 ^{0}C in a MFEC reactor compared with packed-bed reactor in the experimental study of FT reaction. Enhanced heat management enabled the use of reactors with larger diameter in highly exothermic and endothermic reactions.

In contrast with other intensified reactors, commercial catalyst particles can be deposited in fibrous structures. Therefore, Sheng *et al.* [74] proposed microfibrous reactor as feasible solution for heterogeneously catalysed reactions due to easy catalyst loading. However, MFEC is still a developing technology with research needs.

4.3 Catalytic Membrane Reactors

Catalytic membrane reactors include a membrane in the reaction medium. Reversible reactions and their equilibrium limitations may be overcome using this type of reactors. This technology provides reaction enhancement by combining two different approaches. On the one hand, it is possible to control reactants supply or products removal, to or from the reacting medium. Moreover, active sites of the catalyst can be placed on the membrane surface or within the skeleton. As a result, selective membranes can act as a catalyst support with high surface area [50].

In membrane reactors, the reaction occurs at the same time that the membrane selectively permeate desired components according to the partial pressure. This arrangement, shown in Figure 4.5, allows shifting the equilibrium towards desired products [49].

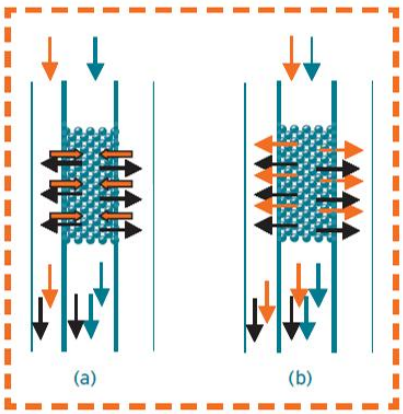

Figure 4.5: Controlled feed (a) and product removal (b) in a non-selective membrane reactor [50].

Integrated sorption-reaction increase the production efficiency. Schlereth *et al.* [25] modelled carbon dioxide methanation to manufacture synthetic natural gas in fixed-bed membrane reactor. CO_2 and H_2 were separately fed to the reaction medium through a steel membrane which allowed good temperature control. The results encourage to develop this technology. However, mass transfer resistance in the fixed-bed must be optimized.

Based on the Le Chatelier 's principle, higher yield is obtained by removing the reaction products which switch the equilibrium towards the forward reaction. In that regard, presence of water in the reaction medium slows down the methanation rate [23]. Ohya *et al.* [26] suggested a membrane for water vapor permeation with integrated ruthenium catalyst. Compared

with conventional reactors, an increase of 18% in the methanation conversion was achieved with the water permeselective membrane reactor. Analogously, improvement was demonstrated by Lebasrbier *et al.* [78] in CH_4 production combining CO methanation with water gas shift reaction (WGS) and CO_2 removal. The sorbent 68%$CaO/MgAl_2O_3$ was impregnated with nickel-based catalysts. Separating one of the reaction products favoured the forward WGS, which led to higher CH_4 yield. Moreover, Miyamoto *et. al* [24] combined CO_2 methanation with NH_3 decomposition in a membrane reactor. The palladium membrane deposited on γ-Al_2O_3 support was located in the reactor along with the Ru/Al_2O_3 catalyst. The hydrogen obtained from the NH_3 decomposition was selectively separated through the palladium membrane to control the H_2 supply for the methanation reaction. As a result, CH_4 selectivity was increased.

Specifications regarding water content in CH_4 streams addressed to the NG network are quite strict (under 90 ppm for Groningen gas grid). Nevertheless, water removal membrane reactor can be utilized to meet these specifications. Walspurger *et al.* [31] proposed carbon dioxide methanation combined with water sorption. They modelled a three reactors system, including in the last reactor a water permeation membrane. As a result, the system soften the severe reaction conditions at which methanation was commonly operated, and enhanced the performance.

The bifunctional membrane concept also enables the separation and conversion of possible impurities present in inlet gases. Hu *et al.* [79] propose an efficient method to eliminate carbon monoxide from H_2-rich streams for further use in proton exchange membrane fuel cells. Platinum membranes involved in proton exchange are highly sensitive to small concentrations of CO impurities. A double functionality palladium membrane with Al_2O_3 supported Ni-catalyst was applied to convert carbon monoxide. Hydrogen was separated at the same time that CO was converted to methane, which avoided membrane contamination.

Perovskite and brownmillerite are ceramics usually used as membranes [30]. Their working principle is illustrated in Figure 4.6. Selective permeation through perovskite membranes allows shifting the chemical equilibrium. This advantage is highlighted when selectivity towards a desired component should be improved. Perovskite materials are able to conduct oxygen and hydrogen ions through their inner crystalline structure at elevated temperatures. Furthermore, perovskite materials were introduced as catalytic components in section 3.4. Additionally, active sites can be fixed to the perovskite surface where catalytic reactions take place. A supplementary function is attributed to perovskite membranes when exothermic and endothermic reactions occur on different sides of the membrane, through which heat is efficiently managed [80].

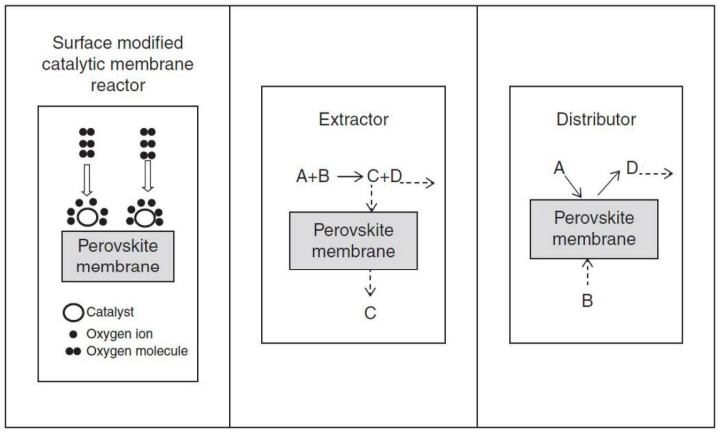

Figure 4.6: Perovskite membrane reactor [80].

Perovskite catalysts have been tested in reaction conditions where other catalysts have failed due to carbon deposition. Jin *et al.* [39] found a good performance for $LaNiO_3$ at high temperatures. Moreover, Dinka *et al.* [47] were able to enhance a variant of perovskite catalyst by using cerium instead lanthanum. This upgrade improved the catalyst behaviour in the presence of sulphur which resulted in a more stable catalyst. However, more effort has to be addressed for the development of perovkite membranes in reactions where certain components or impurities, such as sulphur or steam, disturb their normal operation [80].

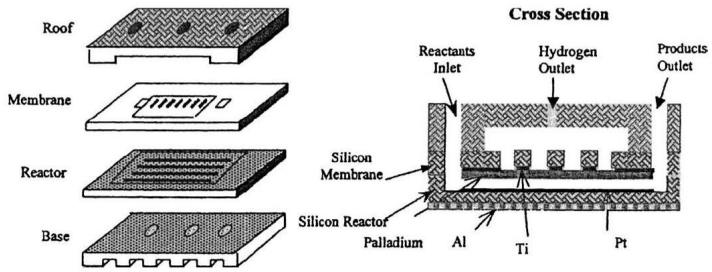

Figure 4.7: Membrane microreactor [80].

Additionally, microreactor and membrane reactor technologies can be combined following the process intensification concept. Kolb *et al.* [27] reported two authors (Zheng *et al.* [81] and Cui *et al.* [82]) who developed membrane reactors for cyclohexane dehydrogenation. An scheme of the membrane microreactor is presented in Figure 4.7. The reactor consists of microchannels loaded with Pt-catalyst. The other structural part is a palladium mem-

brane responsible for hydrogen removal. The Pd-membrane enhances the reaction conversion by means of reducing the thermodynamic limitations of that reaction [80].

4.4 Heat Exchanger Reactors

Heat exchanger (HEX) reactors are heat exchangers where chemical reactions take place. Compared with conventional reactors, some representative improvements in HEX reactor are compactness, heat control, and reaction performance. This type of reactor present characteristics similar to the intensified reactors described until now in Chapter 4 [55]. Furthermore, the three reactor systems, microchannel, structured and catalytic membrane reactors can be implemented in HEX reactors.

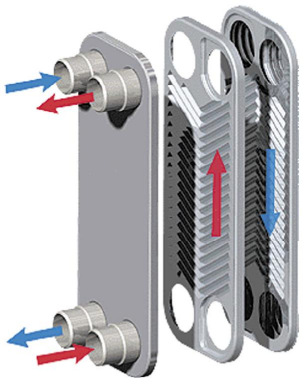

Figure 4.8: Plate heat exchanger-reactor [55].

Heat exchanger reactors may be considered as an alternative to batch reactors, typically used in pharmaceutical and fine chemical industries. Heat exchanger reactors could increase production capacity by working in continuous mode. Furthermore, energy and cost optimization are advantages derived from heat and mass transport intensification which result in higher selectivity and yield. Plant size reduction and increased safety are also positive features of heat exchanger reactors [83]. Additionally, HEX reactors may achieve heat transfer efficiency twenty times higher [84], and operation times ten times shorter than conventional batch reactors [85].

Park *et al.* [86] proposed the use of a heat exchanger reactor loaded with metallic foam washcoated with cobalt-based catalyst for the FT reaction. They obtained efficient heat management, and consequently, control of product distribution was improved. This improvement was promoted by

the construction material of the HEX plates, silicon carbide, with appropriate heat transfer coefficient [87].

In spite of the reaction enhancements achieved with HEX reactors, high surface area and easy loading of packed-bed reactors are still unreachable features for heat exchanger reactors. Brooks *et al.* [22] developed a microchannel HEX reactor in which the Ru-TiO_2 catalyst is coated in a separated metallic sheet. A similar configuration was also validated by Mbodji *et al.* [88] (Figure 4.9). However, the challenges regarding deposition of solid catalyst causes delaying in a wide large scale launch of heat exchanger reactors. Nevertheless, there is a considerable number of companies developing this type of intensified reactors for industrial scale applications [89, 90].

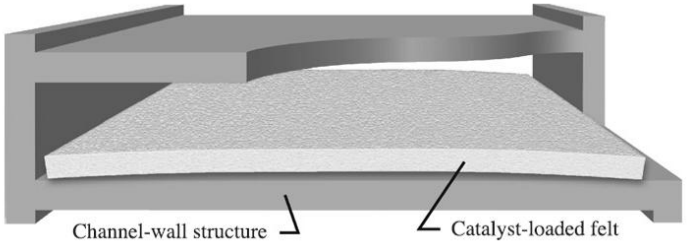

Figure 4.9: Single channel with a interior metal coated place [22].

Chapter 5

Materials and Methods

Carbon dioxide methanation was the target reaction of the experimental work conducted for this thesis. This reaction was performed at various operation conditions over different catalysts in laboratory scale. The objective was to compare the behaviour of novel catalysts with conventional catalysts.

The main topics introduced in this chapter are the experimental set up of the reaction system, analysis methods, execution of the experiments, calculation methods and design of experiments. These subjects will be reviewed in depth to facilitate the interpretation and understanding of the results of the experimental work.

5.1 Experimental Set up

Reactor intensification was a features pursued in this research. Accordingly, the reactor design aimed efficient heat removal and compact size. The reactors were tubes of alloy Inconel 6XI (Figure 5.1), 29 mm long, with inner diameter of 4mm, and 2 mm thick reactor wall.

The experimental set up (Appendix A) comprised a maximum of five reactor tubes placed in parallel (Figure 5.1 (a)). Different catalysts were tested in an overall amount of twenty one reactors. Therefore, the reactors of the experimental set up were changed along the experimental work, which resulted in five different set ups. The five reactors of set up I were washcoated with different contents of catalyst. The second set up had three nanocoated reactors with different contents of catalyst, one washcoated reactor, and one blank. Set up III included reactors coated with washcoats of catalyst and catalyst support, nanocoated catalyst, and a packed-bed reactor. In the set up IV four washcoated reactors were installed. Set up V had two

packed-bed reactors, one of which included the-blocks-and-fins structure. This structure modified the external surface area of the reactor. Figure 5.2 shows the details of the structure consisting of interleaved brass blocks and copper fins. This blocks-and-fins design aimed to intensify heat transfer in a packed-bed reactor. Appendix B presents a table with the reactors installed in of every set up. This table indicates the nickel content of the catalysts and the loading technique utilized in the reactors tested at certain temperature and flow rate set point.

Figure 5.1: Reactor tubes. (a) Reactors installed in the set up, including resistors and thermocouples. (b) Single reactor.

The reactors were operated as individual units. In other words, methanation occurred in one reactor at a time. Once the reactors of a set up were tested, these were changed for new ones. Thus, having up to five reactors in each set up enabled to save time on building up and down activities carried out to change the reactors. In addition, up to five reactors per set up were available to be operated. This was a versatile configuration that streamlined the experimental work.

Heat was supplied to the system through heating elements. On the one hand, heaters were used for tracing the inlet and outlet lines (M-T-135 and

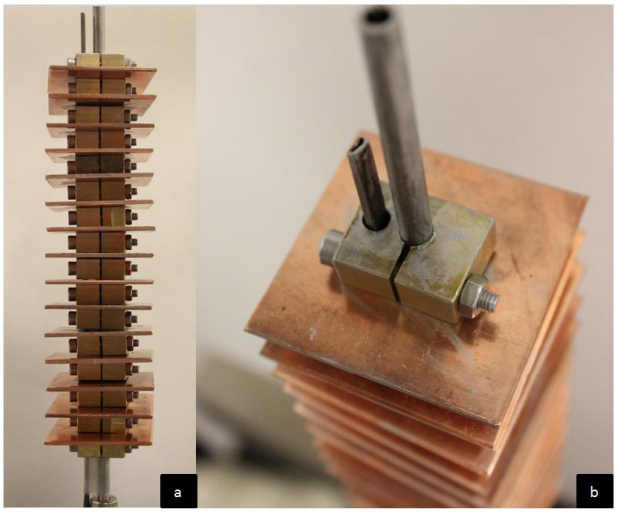

Figure 5.2: Reactor with block-and-fins structure (a) Front view.(b) Section view.

M-T-180 in Figure 5.3). The heating elements were set at 200 ^{0}C to respectively preheat and gradually cool down the inlet and outlet gases. On the other hand, individual heating elements (Figure 5.1 (a)) were placed in contact with each of the reactors (M-T-132, M-T-130, M-T-134, M-T-136 and M-T-150 in Figure 5.3). The temperature controller regulated the temperature of the heating elements through thermocouples in straight contact with those, placed in the upper section of the reactors. In the blocks-and-fins configuration, the heating element passed through the blocks-and-fins structure Figure 5.2. Moreover, the side-drilled blocks hosted the thermocouples to measure the temperature in the outer wall of the reactor.

The lines were operated with manual valves. The three feeding valves to the mass flow meters were on/off ball valves (M-V-100, M-V-110 and M-V-120 in Figure 5.3). The valves controlling the flow until the condenser were on/off gate valves. These valves controlled the gas flow through by-pass and selected reactor/s. M-V-200 controlled the access of reactants to the system, M-V-222 controlled passing gas through the by-pass line, and M-V-223 controlled the downstream access to the condenser and the gas analysis systems.

Pressure was measured in the system with a pressure gauge meter (M-P-131 in Figure 5.3), placed in the feeding line right before M-V-200 valve. Pressure values indicated by the meter were used for conducting the pressure and leaking tests, and in running mode, to check pressure variations.

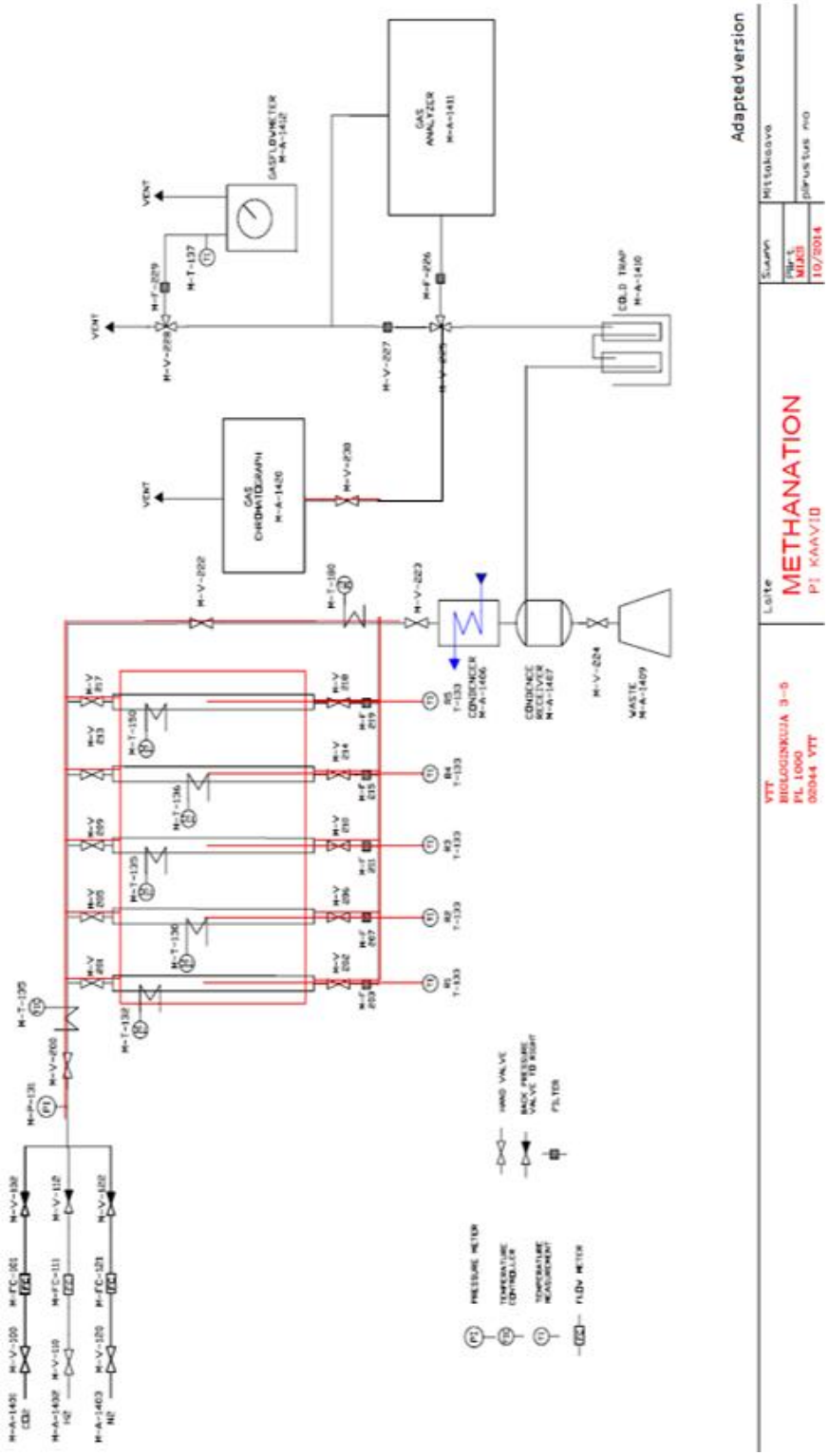

Figure 5.3: Methanation process diagram (by Mari-Leena Koskinen-Soivi, VTT).

The outlet gases passed through a condenser (M-A-1406 in Figure 5.3) downstream the reactors. Consecutively, the gases passed through a pair of cold traps (M-A-1410 in Figure 5.3). Once the water was removed, the flow rate of the dry gas was measured in the gas flow meter (M-A-1412 in Figure 5.3) and subsequently released through the vent. A constant stream of dry gas was withdrawn from the vent line and analysed in the on-line analyser (M-A-1411 in Figure 5.3). Gas chromatograph analysis (M-A-1420 in Figure 5.3) was occasionally performed when more accurate analysis was required.

Inlet flow rate and temperature were the variable experimental parameters. Regarding the inlet flow rate, inert nitrogen and the gaseous reactants, carbon dioxide and hydrogen were fed into the system through mass flow meters, M-FC-101, M-FC-111, M-FC-121 in Figure 5.3. The gas flow was controlled by the flow meter control terminals. The mass flow meters were calibrated to ensure an accurate feeding of the reactants using nitrogen at the beginning of the experimental work. Furthermore, the reaction temperature was measured with thermocouples on the outer wall of the reactors (T-133 in Figure 5.3). The data were collected by the temperature control terminal. The thermocouples were attached to the reactor in straight contact with the external wall, in the front part of these, opposite to the heat source, and close to the mid-section. In some of the reactors the temperature was measured at different reactor heights. In these reactors, several thermocouples were attached at approximately equal distances.

Proper insulation facilities and enhances the heat management. Accordingly, the inlet and outlet lines, and the reactors and thermocouples were wrapped with insulation material in order to control the temperature and minimize heat losses.

5.2 Analysis Methods

ABB on-line analyser AO2000 series, and Hewlett Packard Series II 5890 Gas Chromatograph (GC) analysed the gas compositions. On-line analysers are simple and easy to operate. In addition, this equipment offer accuracy within the range required for this work. Thus, the majority of outlet gases of methanation were exclusively analysed with the on-line analyser. However, several samples were analysed with gas chromatograph when the composition of the gas required more accurate analysis method.

The outlet gases of all the experiments were analysed with the on-line analyser. Furthermore, gas chromatography was additionally applied for those experiments where the inlet flow rate was set under 0,7 ln/min (i.e. 0,3

ln/min), and when the composition of the product was out of the measurement range of the on-line analyser(i.e. $CH_4 < 0{,}1$ vol-%).

5.2.1 On-line Analyser

ABB on-line analyser AO2000 series combine three analyser modules. A glass cell with a thermal conductivity detector measured H_2 in N_2. Oxygen analysis was performed with a thermomagnetic detector. And an infrared photometer analysed CO_2, CO and CH_4. Appendix C includes detailed features of the on-line analyser modules.

The analyser was calibrated to ensure accurate, reliable results prior the beginning of the experimental work and every time the reactors were changed. Zero calibration was made with nitrogen, while the scan calibration was made with two different gas mixtures provided and certificated by AGA OY, composition of which is specified in Appendix C.

5.2.2 Gas Chromatograph Analyser

Hewlett Packard Series II 5890 GC include two analyser modules. A Thermal Conductivity Detector (TCD) analysed H_2, CO_2, CO and N_2. And methane analysis were performed by a Flame Ionization Detector (FID). The gas chromatography column is packed with Carboxen 1000 with 60-80 mesh. The dimensions of the stainless steel column are 1.5 m x 1/8 inch x 2 mmSS (length x outer diameter x inner diameter).

The gas chromatograph was calibrated every time after the stand-by mode was turned off, before the first analysis in order to obtain accurate, reliable results. The calibration gas composition provided and certificated by AGA OY is specified in Appendix C.

5.3 Execution of Experiments

The experimental work was carried out for approximately 13 weeks. Catalyst loading, set up building and modification, and test runs were the main tasks accomplished during the experimental work conducted for this thesis.

Building activities included the initial construction of the experimental set up, and reactor changes for the different set ups (set up I-V). After the reactors were assembled, the heating elements, and control and measurement

thermocouples were attached to the reactors. Subsequently, the system was insulated, and pressure and leaking tests were performed.

Before the test runs, the reactors were flushed with nitrogen to maintain inert environment inside these which avoids undesired reactions. The test runs, involving reduction and reaction, were performed in one reactor at a time.

5.3.1 Catalyst Loading

This work tested nickel-based catalysts on metal oxide supports loading with packed-bed, washcoating and nanocoating techniques. Washcoated catalyst was intended to intensify the heat control in the reactor. Thus, this type of catalyst was the main focus of the experiments.

Packed beds were approximately fixed in the mid-section of the reactors over a quartz wool layer which held the catalyst particles. Figure 5.4 shows a scheme and includes a table with measures regarding location and weight of the catalyst. The packed beds were deposited in the reactor in two different forms. In set up III the bed exclusively consisted of supported nickel catalyst. On the other hand, the catalyst was 50 w-% diluted with silicon carbide in the reactors of set up V. The particles of SiC had similar diameter (300-355 μ-m) to the particles of catalyst (200-300 μm) in order to achieve a more homogeneous dilution (Appendix B).

The washcoated catalyst was applied fully covering the inner wall of the reactors. On the other hand, the nanocoated catalyst was deposited in advance on metallic sheets (Figure 5.5). Thus, tailored pieces were cut from the nanocoated sheet, and rolled and packed in the reactor fully covering the inner surface of the reactor. More detailed information and features of the coating methods are out of the scope of this work.

5.3.2 Reduction of Catalysts

Catalyst activates when the metal oxide of the catalyst is reduced to metal with hydrogen at high temperature. Several authors have studied characterization of nickel-based catalysts with H_2 Temperature-Programmed Reduction (TPR) method [17, 91]. This characterization method provides information regarding the most suitable conditions for proper catalysts reduction. In accordance to those studies, the catalysts were reduced for 2 hours at temperatures between 490 and 600 ^{0}C (variable along the reactor length), atmospheric pressure, and flow rate of H_2:$N_2 = 1$ equal to 1 ln/min.

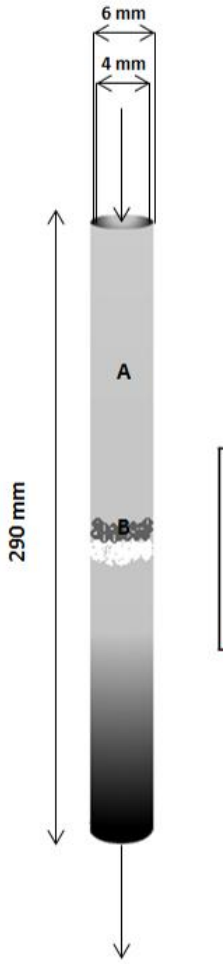

	SIII_R3	SV_R2	SV_R5
A (mm)	130	163	162
B (mm)	15	13	14
mNi (g)	18.15	15.30	15.45
SiC (w-%)	-	50	50

Figure 5.4: Packed bed placement and nickel/SiC contents in set ups III and V, in reactors 3, and 2 and 5 respectively.

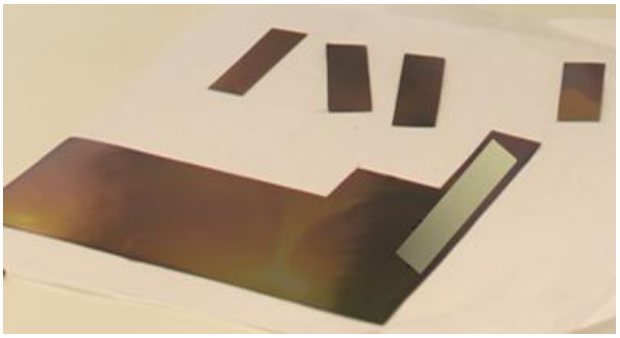

Figure 5.5: Nano-coated metallic sheets.

The reactor with the blocks-and-fins structure had difficulties to reach the reduction temperature established for the other reactors. Therefore, the reactors tested in set up V were reduced for 2 hours at temperatures between 490 and 560 ^{0}C (variable along the reactor length), at the same pressure and flow rate than the other reactors. According to the temperature range favourable for reduction in previous studies [17, 91], these catalysts are not expected to show noticeable differences in the performance.

After the reduction, the reactor was flushed with N_2. An inert environment was maintained in the reactor to avoid the deactivation of the catalyst and other undesired reactions during standby mode.

5.3.3 Reaction

Methanation was performed applying different set point conditions. The temperature range at which the experiments were conducted was selected according to own thermodynamic calculations and, thermodynamic studies [91] and experimental studies [15, 17] found in the literature. The catalysts were tested at three different temperatures (350, 400 and 500 ^{0}C), with three different flow rates at each temperature (0.7, 1 and 1.3 ln/min), H_2:CO_2 = 4 ratio, and at atmospheric pressure. Exceptionally, some of the catalysts were tested at different temperature and flow rates set values. Appendix B summarizes the set points of all the experiments conducted during this experimental work. Moreover, this appendix also includes the type and nickel content of the catalyst tested in each experiment.

The average length of the runs was approximately 30 minutes. This time was enough in most of the runs to achieve constant composition of the outlet gas. In addition, several longer runs were performed over night (10 to 15 hours) to evaluate stability of the catalysts.

After the reaction, the reactor was flushed with N_2. An inert environment was maintained in the reactor to avoid the deactivation of the catalyst and other undesired reactions during standby mode.

5.4 Calculation Methods

Presenting and interpreting results requires representative parameters to assess the performance of the different catalysts. CO_2 conversion (X), CH_4 and CO selectivity (S), and CH_4 yield (Y) were selected for the purpose of catalyst evaluation. Data collected from the analysis methods introduced in Section 5.2 were used for the calculation of those parameters.

The analysis equipment provided the composition of outlet dry gas in volume percentage units (v). These data and the inlet and outlet volumetric flow rates (Q) were used to calculate the values of conversion (Equation 5.1), selectivity (Equation 5.2 and Equation 5.3), and yield (Equation 5.4). It was assumed that $p \cdot R \cdot T_{in} \approx p \cdot R \cdot T_{out}$ in order to be able to use volumetric flows for the following calculations.

$$X_{CO_2} = \frac{Q_{in} \cdot v_{CO_2,in} - Q_{out} \cdot v_{CO_2,out}}{Q_{in} \cdot v_{CO_2,in}} \cdot 100 \tag{5.1}$$

$$S_{CH_4} = \frac{Q_{out} \cdot v_{CH_4,out}}{Q_{in} \cdot v_{CO_2,in} - Q_{out} \cdot v_{CO_2,out}} \cdot 100 \tag{5.2}$$

$$S_{CO} = \frac{Q_{out} \cdot v_{CO,out}}{Q_{in} \cdot v_{CO_2,in} - Q_{out} \cdot v_{CO_2,out}} \cdot 100 \tag{5.3}$$

$$Y_{CH_4} = \frac{Q_{out} \cdot v_{CH_4,out}}{Q_{in} \cdot v_{CO_2,in}} \cdot 100 \tag{5.4}$$

Flow rate and composition of the product stream are referred to dry gas. The carbon balance in Equation 5.5 was used to calculate the total flow rate of the outlet stream which includes the water content.

$$Q_{in} \cdot v_{CO_2,in} = Q_{out} \cdot (v_{CO_2,out} + v_{CH_4,out} + v_{CO,out}) \tag{5.5}$$

Gas hourly space velocity (GHSV) and nickel-weight hourly space velocity ($W_{Ni}HSV$) were calculated as respectively presented in Equation 5.6 and Equation 5.7. These two variables facilitate the evaluation of the catalyst behaviour in direct relation with the amount of catalyst or total nickel content of the catalyst in the reactor.

$$GHSV = \frac{Q_{in}}{V_{Cat}} \tag{5.6}$$

$$W_{Ni}HSV = \frac{\dot{m}_{in}}{m_{Ni}} \tag{5.7}$$

The theoretical composition of the carbon dioxide methanation in the equilibrium state was obtained in order to know in advance the thermodynamic possibilities and limitations of this reaction. HSC Chemistry 6.1, developed by Outotec, was utilized for this purpose. This software bases the calculations of chemical equilibrium composition on the minimization of Gibb's

energy of all the components participating in the reaction. Based on the interest of this work, the equilibrium composition was calculated at atmospheric pressure and temperature ranging from 200 to 700^{0}C. The result of these calculationsn are presented in Chapter 6.

5.5 Design of experiments

The major focus of this thesis was on washcoated catalyst. Therefore, the largest number of experiments comprised carbon dioxide methanation over this type of catalysts.

Nickel-based packed-bed catalysts have been extensively applied for methanation in previous works [17, 92, 93]. Thus, several test were performed using packed-bed catalyst to compare the results of CO_2 methanation over this conventional catalyst with washcoated catalysts. Additionally, packed-bed catalyst was also applied in the tests conducted with the blocks-and-fins design. Packed-bed reactor was selected in order to try to overcome the major difficulties regarding temperature gradients of this type of catalyst.

Nanocoating applied for catalyst deposition is a novel technology. The results obtained with nanocoated catalyst provided poor comparability with the other catalysts. Therefore, only few test runs were executed. The objective of these experiments was to achieve a better understanding of nanocoated catalyst behaviour and to test the suitability of this novel catalysts for CO_2 methanation.

The total number of experiments were carried out in five different set ups. Each set up had from two to five reactors which were independently operated. Appendix B include a table with all the operating points at which the reactors of each set up were tested. In addition, this table indicates the amount of nickel and the type of catalyst loaded in each reactors.

Chapter 6

Results and Discussion

The objective of the experimental work of this thesis was to evaluate the performance of novel catalysts compared with the conventional ones, and the performance of an intensified reactor for the highly exothermic methanation. This chapter present the results of the most relevant experiments conducted with nickel-based catalyst applied by washcoating and nanocating, and in a packed-bed reactor. Conversion, selectivity and yield, and the effect of the reactor-wall temperature on these were used to compare and evaluate the catalyst performance.

The first two sections of the chapter include information concerning equilibrium and temperature distribution for a better understanding of the results presented in following sections. On the other hand, the core sections of this chapter include the results obtained in the experiments with the different types of catalyst.

6.1 Chemical Equilibrium

Figure 6.1 presents the chemical equilibrium composition of the components participating in the methanation of carbon dioxide. The equilibrium data plotted in this figure was obtained with the HSC Chemistry 6.1 software. CO_2 conversion, CH_4 selectivity and yield, and CO selectivity were plotted using equilibrium data (Figure 6.2).

The equilibrium composition was calculated at atmospheric pressure and H_2 to CO_2 ratio equal to 4. Temperature values were varied within the range from 200 to 700^0C in 26^0C increments. The values of these variables were selected in accordance to the experimental conditions of this work. Furthermore, according to the reactions involved in the mechanism of methane

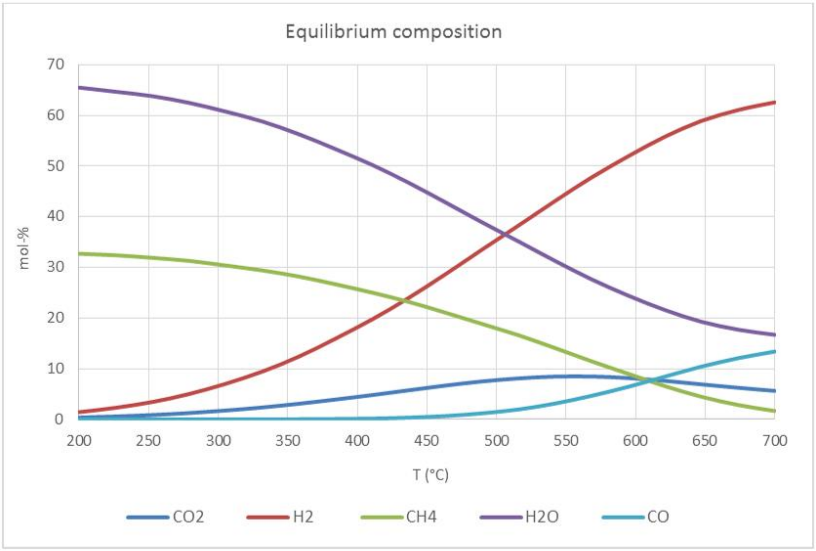

Figure 6.1: Equilibrium composition of species taking part in carbon dioxide methanation at different temperatures.

production (Equation 3.2 and Equation 3.3), the equilibrium mixture consisted of CO_2, CO, H_2, CH_4, and H_2O. HSC Chemistry software calculated the composition of these components at equilibrium based on the Gibb's energy minimization.

Figure 6.1 shows that high temperatures reduces methane production. This is in agreement with the normal behaviour of exothermic reactions. The forward exothermic reaction release heat to the medium. Consequently, the equilibrium is shifted to the backward endothermic reaction to balance the heat released, diminishing the production of methane. Thus, lower temperatures favour the carbon dioxide methanation thermodynamics towards the formation of methane.

Carbon monoxide plays an important role in CO_2 methanation as an undesired side product derived from the reverse water shift reaction (rWSR). CO formation becomes significant at temperatures above 500^0C. As a result, the selectivity towards methane drastically drops (Figure 6.2). This is due to the thermodynamics of rWSR (Equation 3.3), favoured by high temperature.

Several authors reviewed in Section 3.2 focused their research on CO_2 methanation thermodynamics [17, 36, 38]. The most highlighted conclusions extracted from those works matched with the results included in this section. Operation conditions should be maintained at temperatures below 400^0 in order to achieve high CO_2 conversion, and simultaneously maximize the selectivity to methane. According to the thermodynamics, the best results

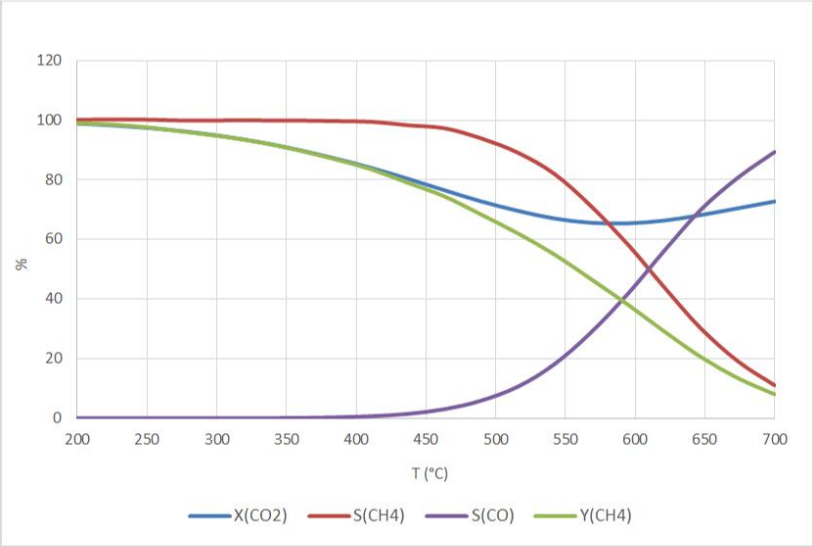

Figure 6.2: Equilibrium CO_2 conversion, CH_4 selectivity and yield, and CO selectivity at different temperatures and 1 bar.

were expected in test runs operated at lower temperatures. Therefore, an active catalyst for methanation was crucial to achieve a good reaction rate.

6.2 Temperature Distribution

Temperature significantly affected the performance of the exothermic carbon dioxide methanation. Thus, the heat released by this reaction had to be effectively removed.

Some general facts must be considered prior to the evaluation of temperature distribution in the reactors. First, it is worth to emphasise that the temperatures presented in the charts correspond to the temperature measured on the outer wall of the reactor. Thus, the actual temperature inside the reactor was considered to be higher. Second, the heating elements which provided heat to the reactors were separate units. Therefore, variations in the heat supply could be assumed between different reactors. Thirdly, the temperature in the top and bottom of the reactors were considerably lower. On the one hand, the inlet stream entered to the reactor preheated at 200^0C. This temperature was lower than any of the temperature set points fixed in the the test runs. On the other hand, the insulation of the heating element tail was insufficient, which resulted in noticeable heat losses. Lastly, the exact location of the catalyst in the packed-bed reactors enables better understanding of the temperature distribution in the reactors. Figure 5.4

schematically showed the placement of the packed-bed catalysts, and in Figure 6.4 and Figure 6.5 the location of the catalyst is highlighted in black.

Four different reactors were considered to analyse the temperature distribution in the axial coordinate of the reactor. Two washcoated reactors with different nickel loading, and two packed-bed reactors 50 w-% diluted with SiC, one of which included the blocks-and-fins structure (Figure 5.2). Figure 6.3 shows the temperature distribution along the four reactors previously described. The temperature set point was equal to 350^0C in every case.

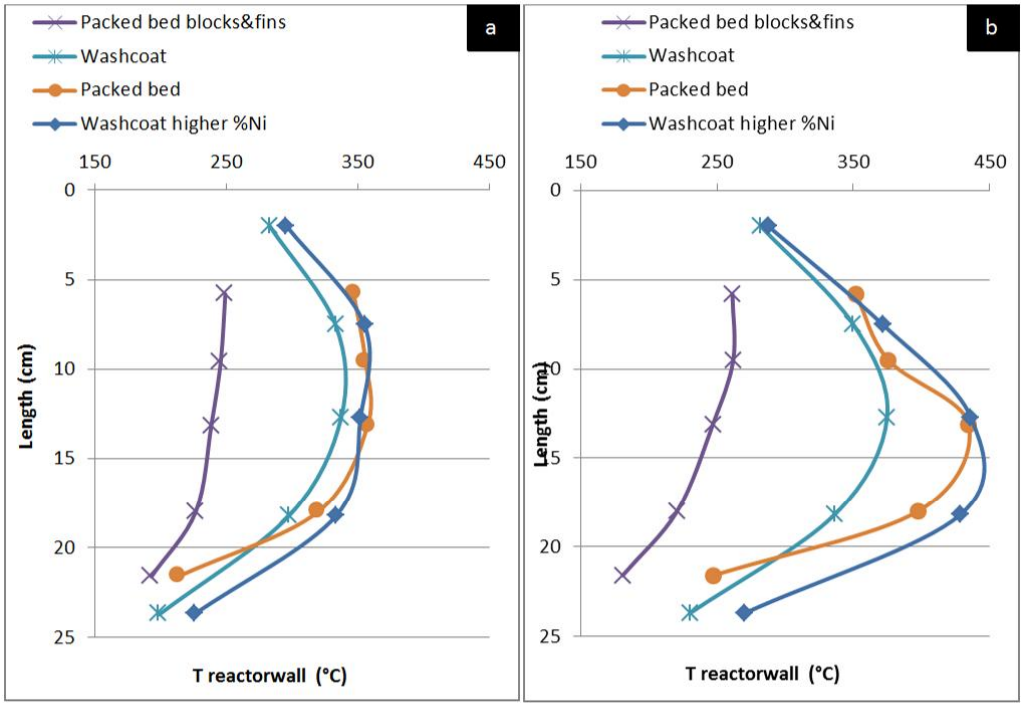

Figure 6.3: Temperature on the outer wall along the reactor length with temperature set point equal to 350^0C and inlet rate equal to 1.0 ln/min of (a) inert nitrogen and (b) reactants (H_2:CO_2 = 4). Violet: m_{Ni}=15.4mg, light blue: m_{Ni}=16.8mg, orange: m_{Ni}=15.3mg, dark blue: m_{Ni}=33.8mg.

Figure 6.3 (a) presents the temperature profile of the reactors fed with inert nitrogen. In this comparative case, only the heating elements and the blocks-and-fins affected the temperature measured along the reactor wall. The washcoated reactors and the packed-bed reactor showed similar heat distribution. Both types of reactors exhibited good control of the temperature close to the set point only in the mid-sections. On the other hand, the packed-bed reactor with blocks-and-fins structure presented considerably different temperature profile. The temperature was more homogeneous along the reactor length. However, efficient heat removal of the blocks-and-fins design resulted in inefficient heat control. Consequently, the tempera-

ture of the reactor wall (between 200 and 250^{0}C) remained under the set point value.

Figure 6.3 (b) shows the temperature profile when methanation was taking place. Therefore, in this chart the catalyst loading technique introduced variations in the heat distribution, in addition to the differences already found in Figure 6.3 (a). The packed-bed reactor with the blocks-and-fins structure hardly reached the minimum temperature for the activation of the catalyst. CO_2 conversion was 0.5%, and thus, the curve barely varies. In contrast, the washcoated with higher percentage of nickel and the other packed-bed reactor exhibited a significant influence of the exothermic methanation on the temperature distribution. The former reactor was loaded with double amount of nickel than the rest of reactors. Increasing the amount of nickel improves the reaction rate. Therefore, the higher amount of heat released by the exothermic reaction resulted in a 100^{0}C increment of temperature on the reactor wall with regard to the set point. The packed-bed reactor with only 15.3 mg of nickel achieved similar temperature due to hot-spot formation and inefficient heat transfer of this type of reactors. Conversely, the washcoated reactor with 16.8 mg of nickel showed efficient heat removal. This facilitated maintaining the reactor temperature close to the set point.

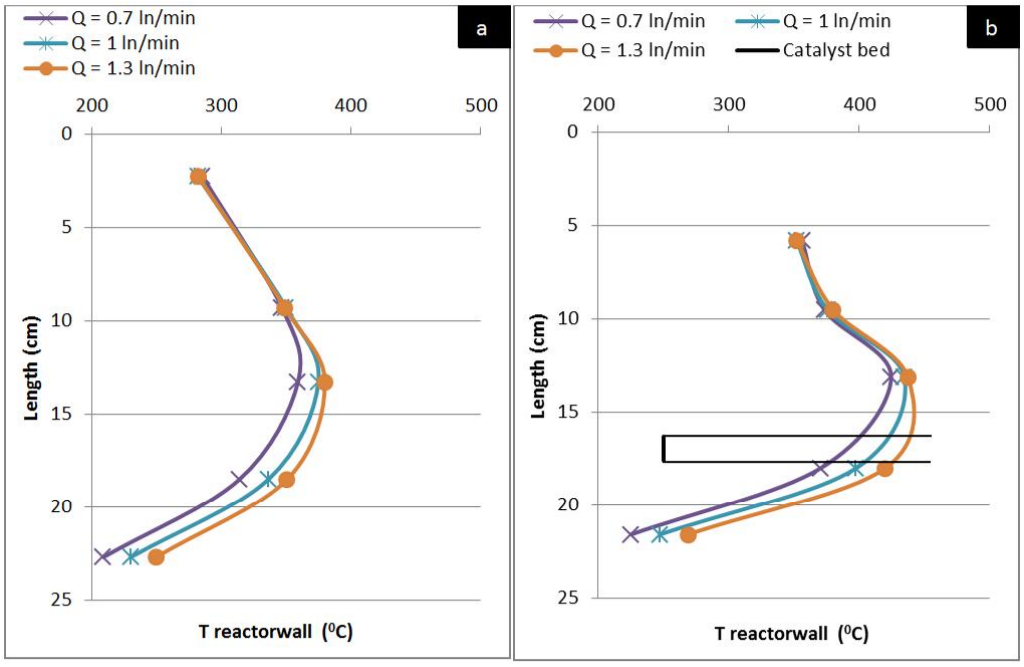

Figure 6.4: Temperature measured on the outer wall along the reactor length. Set point temperature at 350^{0}C. (a) Washcoated catalyst (m_{Ni}=16.8mg). (b) Packed-bed catalyst (m_{Ni}=15.3mg).

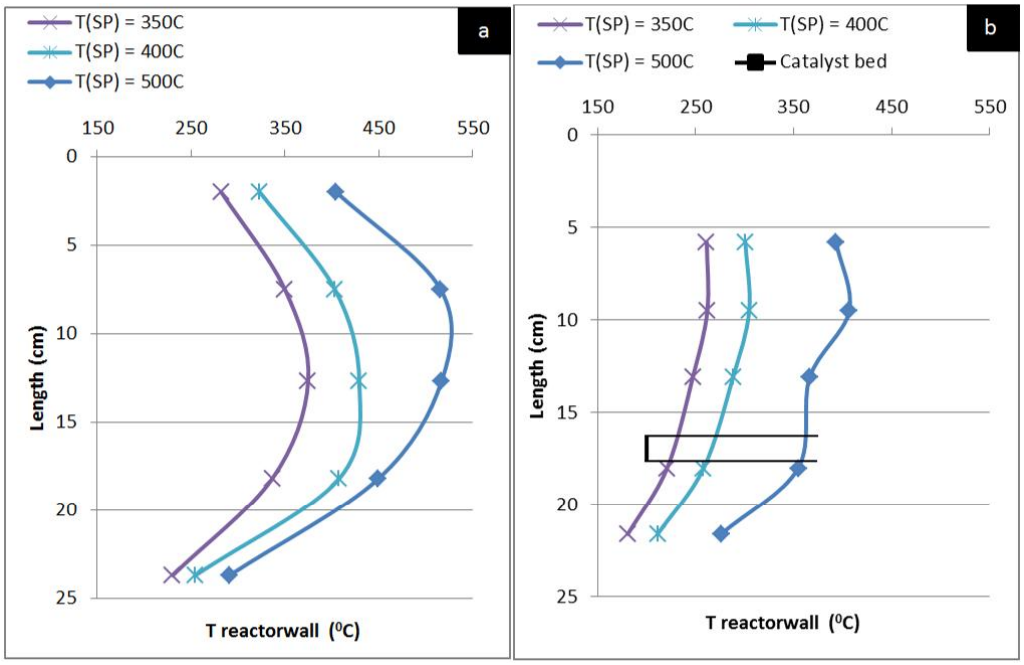

Figure 6.5: Temperature measured on the outer wall along the reactor length. Inlet rate equal to 1 ln/min. (a) Washcoated catalyst (m_{Ni}=16.8mg). (b) Packed-bed catalyst (m_{Ni}=15.4mg) with blocks and fins structure.

Figure 6.4 shows the temperature distribution of (a) the washcoated reactor and (b) the packed-bed reactor with similar amounts of nickel. Higher flow rates resulted in higher temperature due to increased amount of reactants fed into the reactor, which increased the amount of heat released. However, lower flow rates favoured higher conversion which increased the temperature. However, the extent of the reaction had more effect over the absolute heat released than conversion. The temperature set point was for both reactors 350^0C. However, the heat released by methanation increased the reactor temperature. The washcoated reactor represented in chart Figure 6.4(a) exhibited a soft curve with values under 400^0C. On the other hand, chart (b) shows a sharper curve with values above 400^0C in the hottest points near the location of the catalyst bed. Thus, the heat released by the exothermic methanation was quickly removed when a thin washcoat was applied. In contrast, the hot-spots in packed-bed catalyst increased the temperature in the mid-section of the reactor. Nonetheless, the temperature at the exact location of the packed-bed decreased because of simultaneous axial heat conduction and heat losses through the insulation. This comparison evinced a clear advantage of washcoated catalyst in temperature control due to lower bulk density of the catalyst in the tube. Improvements in the performance of washcoated catalysts was already proved in other reactor

configurations for thermally demanding reactions [61, 62].

Several experiments were carried out at different temperature set points (350, 400 and 500^{0}C) to compare the temperature distribution in (a) a washcoated reactor and in (b) the packed-bed reactor with the blocks-and-fins structure. Figure 6.5 shows the results of those experiments conducted with inlet flow rate of 1 ln/min. The increased surface area of the blocks-and-fins design facilitated heat removal. Consequently, the blocks-and-fins structure required higher heat supply than the washcoated reactor to reach certain temperature. Hence, the actual operation conditions were far from any temperature set point established. In spite of the higher energetic needs, this design provided good heat management. As a result the temperature along the reactor wall was quite homogeneous.

6.3 Experiments with Packed-bed Catalyst

Three different packed-bed reactors were tested: a reactor with commercial catalyst, and two packed-beds of the same commercial catalyst, diluted with 50 w-% SiC. One of this two was packed in the reactor with the blocks-and-fins structure.

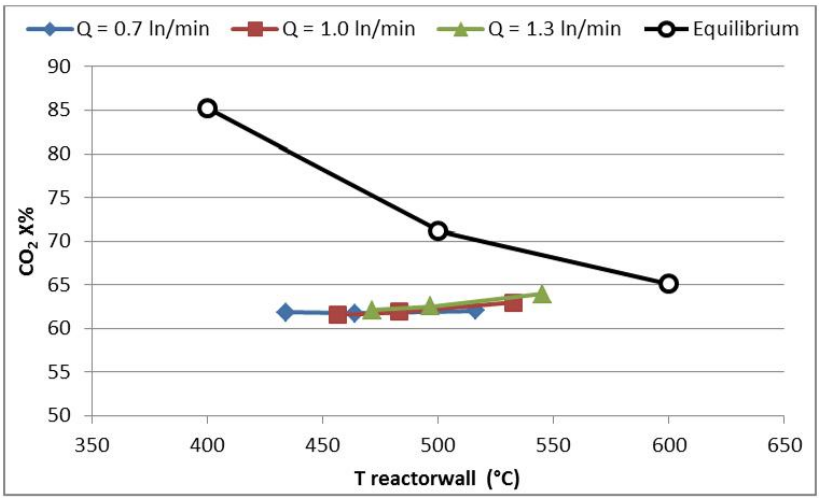

Figure 6.6: Effect of the reaction temperature on the CO_2 conversion of methanation for different inlet flow rates. Results from packed-bed reactor with 18.2 mg of nickel content.

Figure 6.6 shows the conversion of the packed-bed reactor. Conversion exhibited almost no variation at different flow rate and temperature set

points. Therefore, chemical equilibrium can be assumed. The temperature measured in the reactor wall was lower than in the core of the catalyst bed. Furthermore, Figure 6.6 shows different conversion values at theoretical equilibrium, represented as the black curve.

Table 6.1 shows the conversion and selectivity obtained with the packed-bed and diluted packed-bed reactors. In spite of the virtually constant conversion, the selectivity was notably affected by temperature variations, which can be also seen in Figure 6.7. Methane (Figure 6.7(a)) and carbon monoxide Figure 6.7(b)) selectivities followed the trends reported in the literature [17, 36], and were in agreement with the equilibrium results presented in section 6.1. In accordance to the chemical equilibrium, carbon monoxide concentration begins to be noticeable when methanation is carried out at temperature above 500^0C. Lower temperatures promoted methane production, improving the selectivity towards this component. Conversely, higher temperatures favoured the endothermic rWSR which increased CO selectivity. Additionally, increases in the inlet flow rate rose the temperature in the reactor. As a result, the CH_4 selectivity was lower. Furthermore, the selectivity was lower in the experimental results than the values predicted by the equilibrium calculation. The difference of temperature between the catalyst bed and the external wall of the reactor were assumed to be significant. Accordingly, selectivity represented in Figure 6.7 correspond to selectivity values usually found at higher temperature. For instance, the equilibrium selectivity of methane was around 80% at temperature under 500^0C, while the experimental results achieved approximately 50% selectivity.

Catalys	T (^{0}C)	Q_{in} (ln/min)	CO_2 X%	CH_4 S%
18.2 PB	434.2	0.7	61.9	77.0
	456.6	1.0	61.6	66.2
	471.3	1.3	62.1	60.1
	464.0	0.7	61.7	70.9
	483.3	1.0	62.0	60.6
	496.8	1.3	62.6	54.6
	516.4	0.7	62.5	56.0
	532.5	1.0	63.0	47.4
	545.0	1.3	63.9	42.4
15.3 PB	370.5	0.7	61.8	75.8
	397.7	1.0	61.8	64.5
	420.0	1.3	62.6	58.2
	453.9	2.0	63.9	50.2

Table 6.1: CO_2 conversion and CH_4 selectivity of packed-bed catalysts with 18.2 mg of Ni, and 15.3 mg of Ni diluted with 50 w-% of SiC. Type of catalyst: Packed-bed (PB). Mass of nickel in mg.

Methane yield decreased at higher temperature as a result of lower CH_4 selectivity. Figure 6.8 shows the reduction of methane production at higher temperatures at which the carbon monoxide formation was more favourable.

The performance of nickel-based catalyst in methanation was expected to be good in terms of CO_2 conversion and CH_4 selectivity according to Rahmani

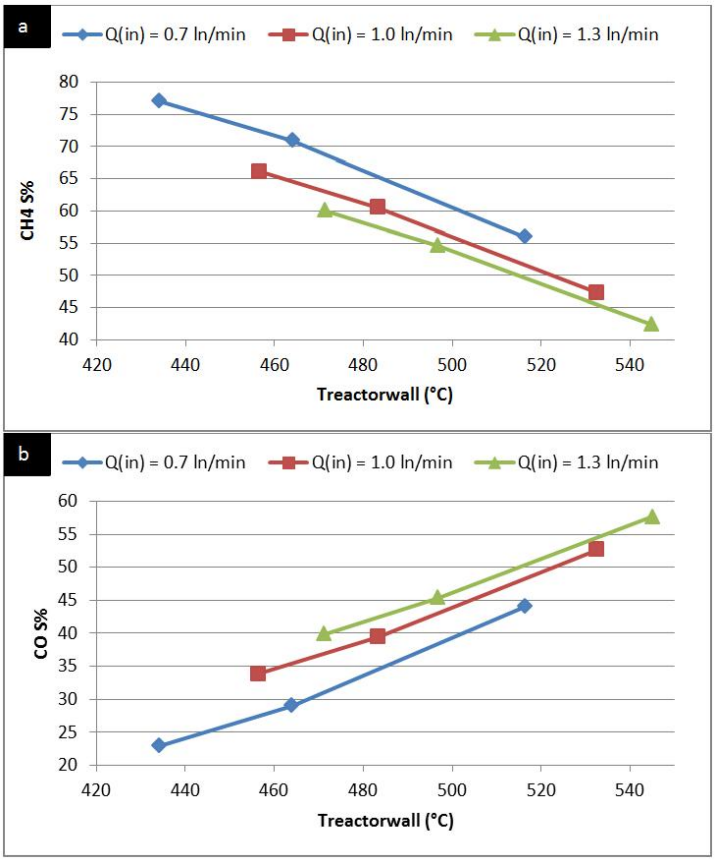

Figure 6.7: Effect of the reaction temperature on the CH_4 (a) and CO (b) selectivity in methanation for different inlet flow rates. Results from packed-bed reactor with 18.2 mg of nickel content.

et al. [17]. They carried out methanation experiments in a fixed-bed reactor of Ni/Al_2O_3 catalyst. Carbon dioxide conversion reached values close to 80% and about 90% of methane selectivity. Garbarino *et al.* [93] conducted methanation experiments over Ni/Al_2O_3 catalyst. They obtained lower conversion equal to 75%, but 100% selectivity towards methane. None of this values were achieved in the experiments conducted for this thesis. The GHSVs applied in the experiments over packed-bed catalyst were between 20000 and 45000 h^{-1}, while Garbarino *et al.* applied 52300 h^{-1}. Furthermore, the experimental results presented in Figure 6.8 were close to the values obtained by Aziz *et al.* [15] with CO_2 conversion up to 64.1% over fixe-bed of Ni/MSN catalyst. Similar value of conversion was also achieved by Chang *et al.* [92] over nickel-supported on rice husk ash-alumina ($Ni/RHA\text{-}Al_2O_3$). However, the CH_4 selectivity reached in the experiments performed for this thesis is considerably lower (under 80%) than in the works reviewed in the literature.

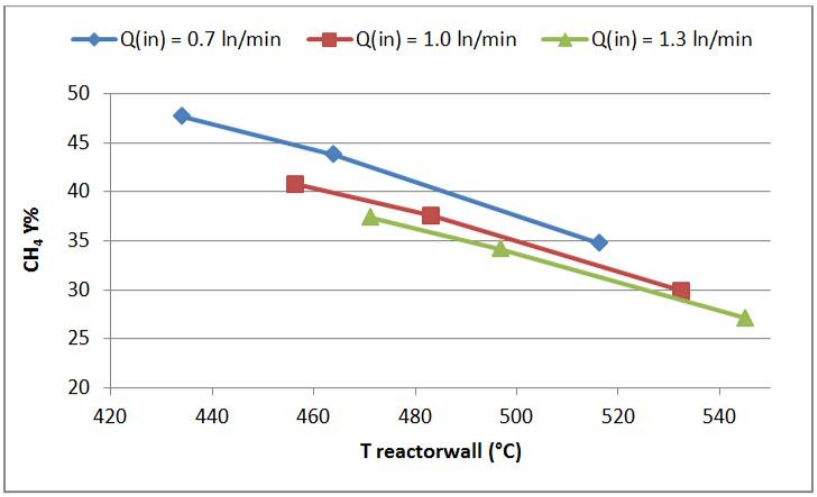

Figure 6.8: Effect of the reaction temperature on the CH_4 yield in methanation for different inlet flow rates. Results from packed-bed reactor with 18.2 mg of nickel content.

The experiments conducted in the diluted packed-bed reactor resulted in similar values of conversion, selectivity and yield as for the packed-bed reactor. On the other hand, the results from the experiments carried out in the diluted packed-bed catalyst loaded in the blocks-and-fin reactor were noticeably different. Figure 6.9 shows (a) the CO_2 conversion and (b) CH_4 selectivity. The comparison of these systems is challenging due to different range of operation temperature in the reactors. The blocks-and-fin reactor worked at lower temperature than the packed-bed reactor. Lower temperature resulted in lower reaction rate. Nevertheless, the diluted packed-bed catalyst achieved similar conversion in the block-and-fins-reactor as the packed-bed reactor. In addition, the selectivity improved a 10% in the blocks-and-fins reactor due to the heat removal ability of this reactor. For instance, the packed-bed reactor reached temperatures close to 550^0C while the blocks-and-fins reactor worked at 360^0C when the temperature set point was 500^0C.

6.4 Experiments with Washcoated Catalyst

The nickel content of the washcoated catalyst was different in each of reactors tested in the experiments. The amounts of nickel varied form 5 to 70 mg approximately. Furthermore, the nickel percentage was the same in all the catalysts, on the level of nickel-based catalyst typically used in reforming reactions, except for one of the catalyst. This catalyst contained a

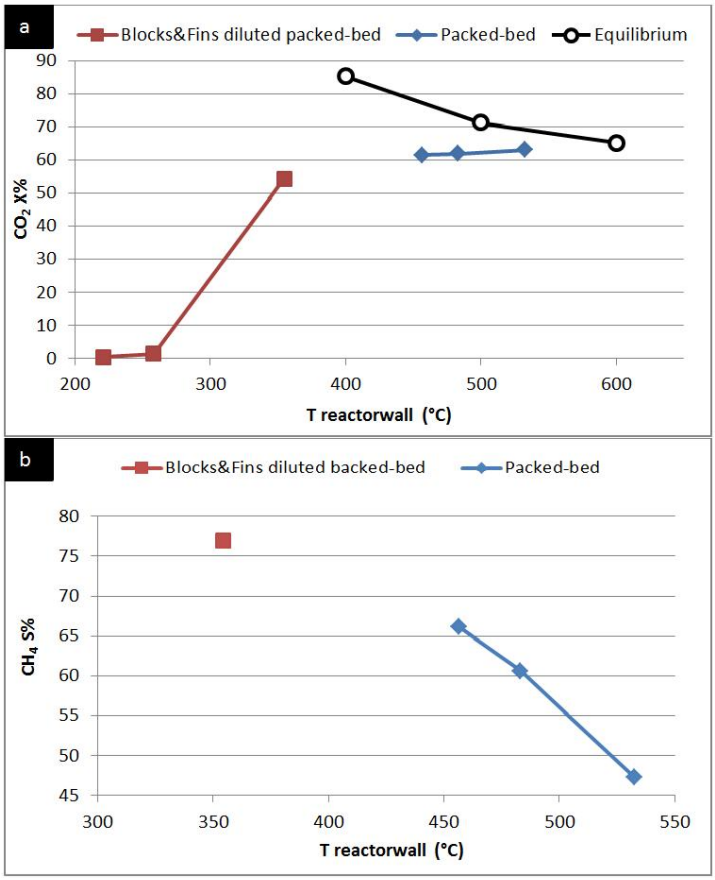

Figure 6.9: Effect of the reaction temperature on the CO_2 conversion (a) and CH_4 selectivity (b) in methanation for different reaction systems with similar amount of catalyst, and inlet flow rate equal to 1 ln/min and set point temperature equal to 500^0C. Results from diluted packed-bed with 15.4 mg of Ni content in the reactor with blocks-and-fins structure, and packed-bed with 18.2 mg of Ni content.

higher nickel percentage, on the level of the nickel-based catalyst typically used for methanation.

In this section, washcoated catalysts are assessed based on three points of view. First, the general performance of washcoated catalyst is analysed in terms of conversion, selectivity and yield. Secondly, washcoats with different nickel contents are compared. Finally, this section includes an evaluation of the stability of different washcoated catalysts.

6.4.1 Catalyst Performance

The performance of all washcoated catalysts samples tested resulted in similar trends on the basis of conversion, selectivity and yield. Naturally, the

absolute values of these parameters varied in accordance with the amount of catalyst loaded in the reactors. The results obtained from the experiments performed with a washcoated catalyst with nickel content equal to 15 mg were used as a representative example of the behaviour of washcoated catalysts.

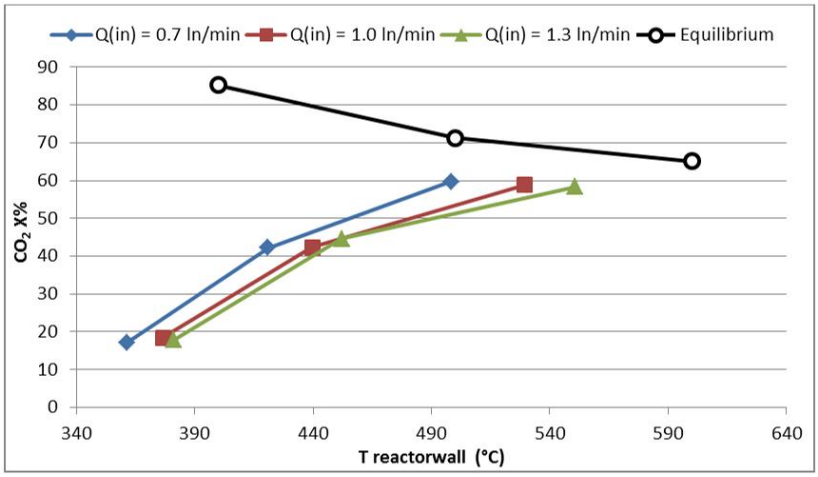

Figure 6.10: Effect of the reaction temperature on the CO_2 conversion in methanation for different inlet flow rates. Results from washcoated reactor with 15 mg of nickel content.

Figure 6.10 shows higher CO_2 conversion at higher temperatures. The rate of methanation increased with temperature. Thus, the greatest conversions were achieved at higher temperature. This behaviour was also found by Garbarino *et al.* [93] in the experimental research of nickel-based catalyst for methanation in a fixed-bed reactor. Carbon dioxide conversion achieved values up to 75% with 100% selectivity towards methane at 500^0C. In comparison, the highest CO_2 conversion achieved over a washcoated catalyst with 69.0 mg of nickel was close to 70%. This value of conversion coincided with the CO_2 conversion in chemical equilibrium at 500^0C. Although the curves representing the experimental results did not reach the equilibrium curve, the reaction was considered to be in chemical equilibrium at temperature close to 500^0C. However, the temperature measurements in the reactor wall showed lower values than the actual temperature within the reactor.

The thermodynamics of carbon dioxide methanation is characterized by high methane selectivity, near 100% at low temperatures and up to 450^0C. Hence, the selectivity at the highest temperatures shown in Figure 6.11 matched with the thermodynamics calculation. On the other hand, at lower

temperatures the reaction was in a regime where the selectivity was determined by the kinetics not by chemical equilibrium. Consequently, methane selectivity decreased at lower temperatures.

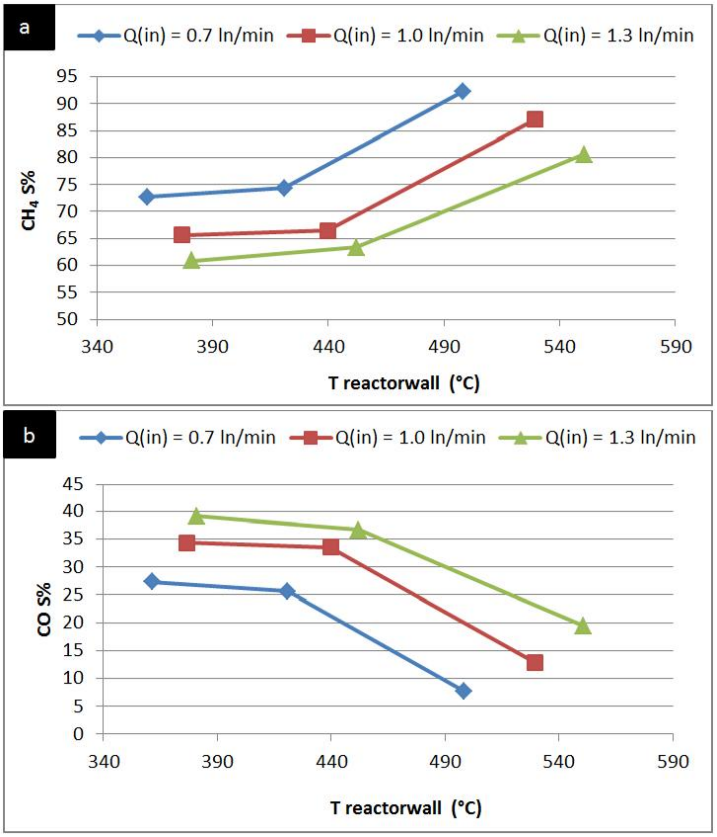

Figure 6.11: Effect of the reaction temperature on the CH_4 (a) and CO (b) selectivity in methanation for different inlet flow rates. Results from washcoated reactor with 15 mg of nickel content.

Yield is a variable directly affected by conversion and selectivity. Accordingly to the trends followed by carbon dioxide conversion and methane selectivity, Figure 6.12 shows increase of yield at higher temperatures.

Washcoating was reviewed in the literature survey of this thesis as a potential catalyst deposition technique applicable in intensified reactors. Tronconi *et al.* [51] evaluated various non-adiabatic reaction systems where washcoating was used for catalyst loading. For instance, monoliths, open-cell foams and micro-fibrous materials were considered as promising structured reactors with advanced features in comparison with conventional reactors. The use of washcoated catalyst was also highlighted by Kolb *et al.* [94] as the most suitable method for catalyst deposition in microchannel

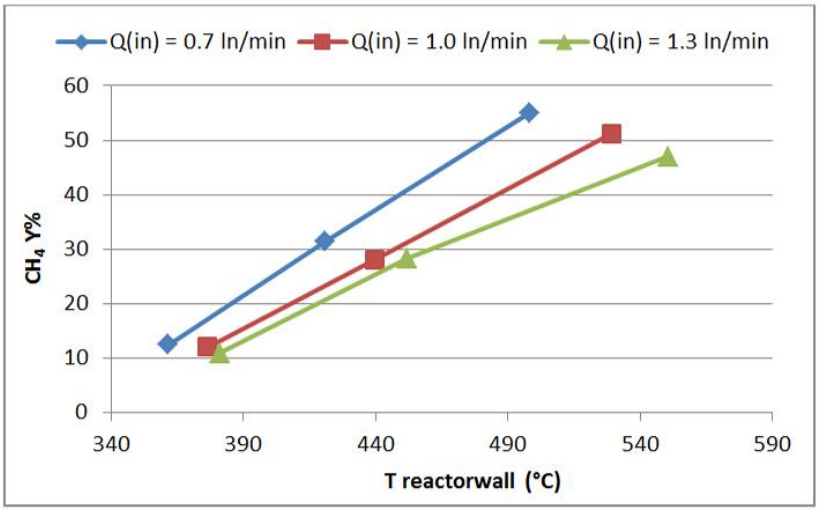

Figure 6.12: Effect of the reaction temperature on the CH_4 yield in methanation for different inlet flow rates. Results from washcoated reactor with 15 mg of nickel content.

reactors. The number of publications regarding washcoating technology is considerably growing. However, no publication has been found regarding nickel-based washcoated catalysts applied for carbon dioxide methanation to compare the results of this work.

6.4.2 Effect of Nickel Content

Samples of washcoated catalyst with nickel mass from 5.3 to 64.4 mg were tested at different operation conditions. The nickel content in the washcoated reactors was evaluated in terms of:

- the effect of nickel content in catalysts with the same nickel loading,
- the effect of nickel content in catalysts with different nickel loading,
- and the repeatability of the experiments with the catalysts with similar nickel content and same nickel loading.

Figure 6.13 shows enhanced carbon dioxide conversion for samples with higher amount of nickel in the catalyst. The conversion improved with higher amount of active metal. Moreover, methanation reached the equilibrium independently of the catalyst used at high temperature, when the set point was fixed at 500^0C. Nonetheless, the experimental conversion curves and the equilibrium curve are spaced some distance apart due to the difference of temperature inside and on the external wall of the reactor.

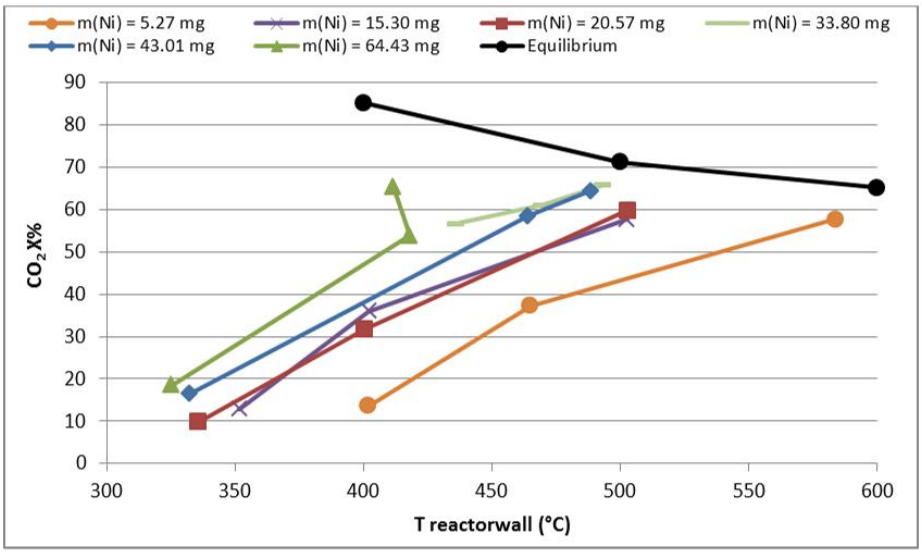

Figure 6.13: Effect of the reaction temperature on the CO_2 conversion in methanation for catalysts with different amounts of nickel content at inlet flow rate equal to 1.0 ln/min.

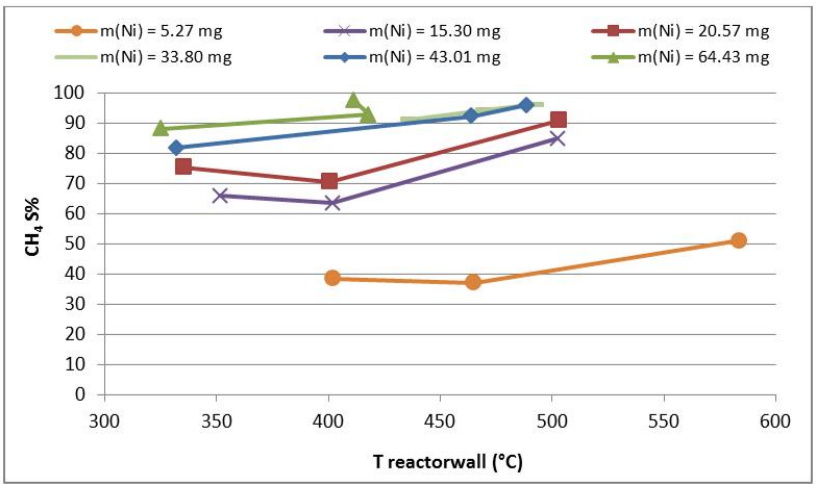

Figure 6.14: Effect of the reaction temperature on the CH_4 selectivity in methanation for catalysts with different amounts of nickel at inlet flow rate equal to 1.0 ln/min.

Selectivity of methane was also improved in the reactors with higher nickel content. Figure 6.14 shows more favourable methane production in the reactors where catalysts with higher content of nickel were applied. Those catalysts with higher mass of nickel, such as 43.0 and 64.4 mg, exhibited

CH_4 selectivities as high as the equilibrium selectivities. Higher number of active sites seem to favour methane over rWSR at operation conditions in which carbon monoxide production become more significant.

The catalyst with content of nickel equal to 33.8 mg achieved better conversion and selectivity compared to the results obtained with the catalyst with more nickel content (43.0 mg). Nonetheless, the former catalyst had higher nickel loading than any of the other catalyst included in Figure 6.13 and Figure 6.14. Consequently, larger proportion of active sites improved the performance of this catalyst. Similarly, Garbarino *et al.* [93] found increased conversion values with catalyst containing higher nickel loading. Moreover, higher activity of the catalysts resulted increased the heat release from the exothermic methantion. Thus, the curve representing the catalyst with 33.8 mg of nickel shows a working range of temperature much narrower than the other catalysts.

The last comparison made in this section concerning nickel content refers to a repeatability study conducted for catalysts with similar nickel mass from 15 to 17 mg. Figure 6.15 shows excellent repeatability of the catalysts with 15.3 and 16.8 mg of nickel. In contrast, the reactor with the 15.0 mg of nickel catalyst exhibited heat control deficiency due to differences in the heat supply of the heating element.

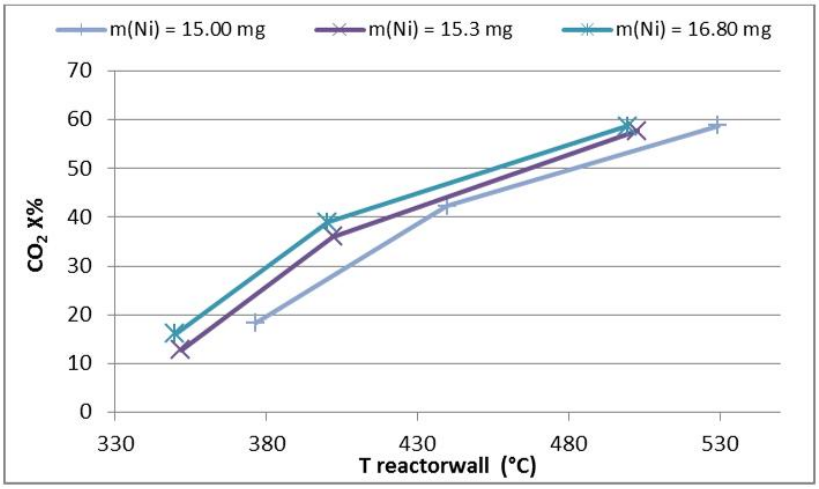

Figure 6.15: Effect of the reaction temperature on the CO_2 conversion in methanation for catalysts with similar amounts of nickel content at inlet flow rate equal to 1.0 ln/min.

6.4.3 Catalyst Stability

The stability of four catalysts were tested in few longer runs. The run times presented in Figure 6.16 are discontinuous. In other words, stand-by stages, and different set points runs occurred among the runs of which data is showed in this figure. Figure 6.16 shows (a) carbon dioxide conversion and (b) methane selectivity obtained from runs at temperature set point of 350^0C and inlet flow rate equal to 1 ln/min. These operation conditions selected to assess the stability of the catalysts were the check set point at the beginning and end of every test run. Thus, the results from check set points and longer, over night run test were used to evaluate the stability of the catalysts. The rest of set points conducted at different temperature and flow rates were not included in the stability charts.

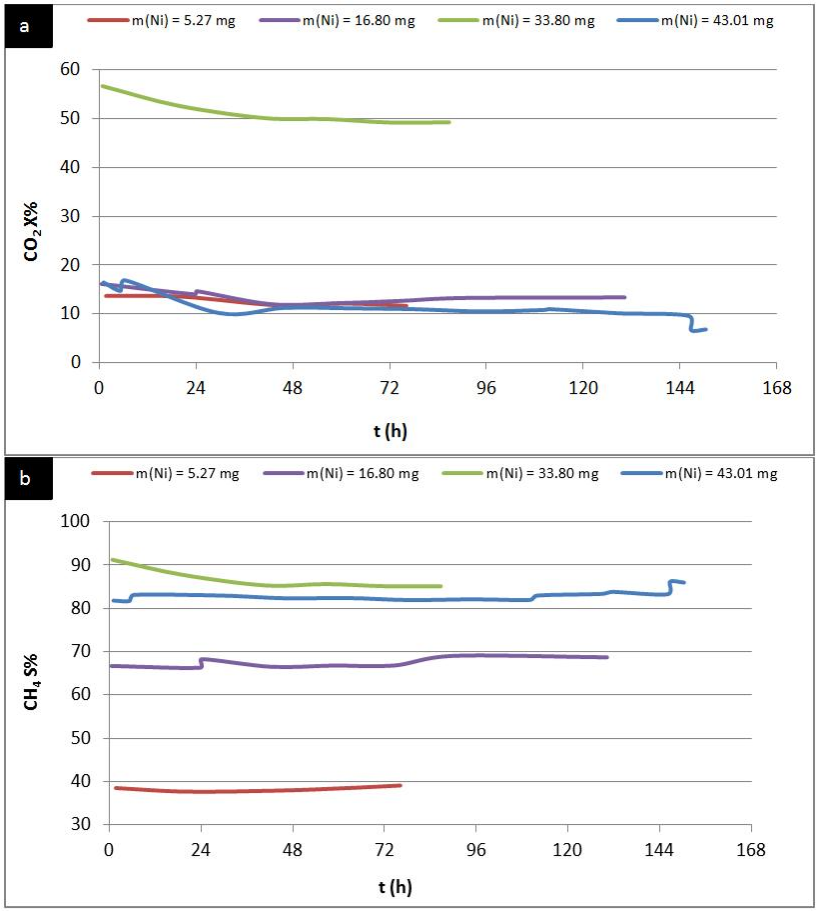

Figure 6.16: Effect of the reaction time on the CO_2 conversion (a) and CH_4 selectivity (b). Results from washcoated reactors with different nickel content in the catalyst.

The catalysts analysed in this section showed good initial stability. After the first 48 hours of test run, almost no change in conversion or selectivity was observed. Therefore, the first 48 hours can be considered as catalytic stabilization period. Furthermore, experiments were performed at higher temperature and different flow rates within that period. Thus, those runs might have affected the initial activity. Table 6.2 shows the variation percentage in conversion and selectivity of catalysts with different nickel contents within the stabilization period. These percentages were calculated considering the 70-80 first running hours of the catalyst.

m_{Ni} (mg)	CO_2 X variation (%)	CH_4 S variation (%)
5.3	14.8	-1.5
16.8	21.6	-0.2
33.8	13.2	6.7
43.0	33.4	-0.2

Table 6.2: CO_2 conversion and CH_4 selectivity variation percentage. Catalysts with nickel contents equal to 5.3, 16.8 and 43.0 mg have lower nickel loading in the catalyst than the one with 33.8 mg.

The catalysts with lower nickel loading had noticeable conversion loss during the stabilization time. These losses were more obvious for the catalysts with higher nickel content. Nevertheless, the selectivity towards methane was improved, presumably due to changes in the active surface or morphology of the catalyst. In contrast, the catalyst with higher nickel loading preserved the carbon dioxide conversion closer to the initial values. However, this catalyst exhibited methane selectivity loss up to 6.70%.

6.5 Washcoated vs. Packed-bed Reactors

Packed-bed reactors were operated in GHSV range between 20000 and 45000 1/h, while the GHSV applied in washcoated reactors was between 1000 and 2000 1/h. The considerable difference in the values of GHSV of the two types of reactors was a consequence of the catalyst dispersion inside the reactor. The pellet beds of the packed reactors were limited to an approximate height of 1.50 cm. Conversely, the washcoats were applied to the entire inner surface of the reactors.

A laminar flow regimen can be assumed in the washcoated and packed-bed reactors due to low flow rates and narrow diameter of the reactors. Thus, temperature and composition gradients might have been present in the radial direction of the fluid. Packed bed reactors had higher surface area. Therefore, the composition gradients were not supposed to be significant. In contrast, diffusion limitations can be assumed at the interface of washcoat

layer, party due to the laminar flow profile. This drawback was observed in the microchannel reactor analysed by Gavriilidis *et al.* [56].

Pressure drop is a major disadvantage in packed-bed reactors [49, 50, 64]. The packed-bed reactors tested in the experiments exhibited pressure drop which varied with different flow rates. At the lowest flow rates the pressure measured in the system was close to 0.2 bar(g) and up to 0.6 bar(g) at the highest flow rates. Conversely, washcoated reactors presented no pressure drop.

In this section, the heat removal and catalyst performance were evaluated and compared for CO_2 methanation conducted in a washcoated and a packed-bed reactors. The reactors selected for this comparative analysis had similar amounts of nickel in the washcoat and the pellet bed, 20.6 and 18.2 mg respectively.

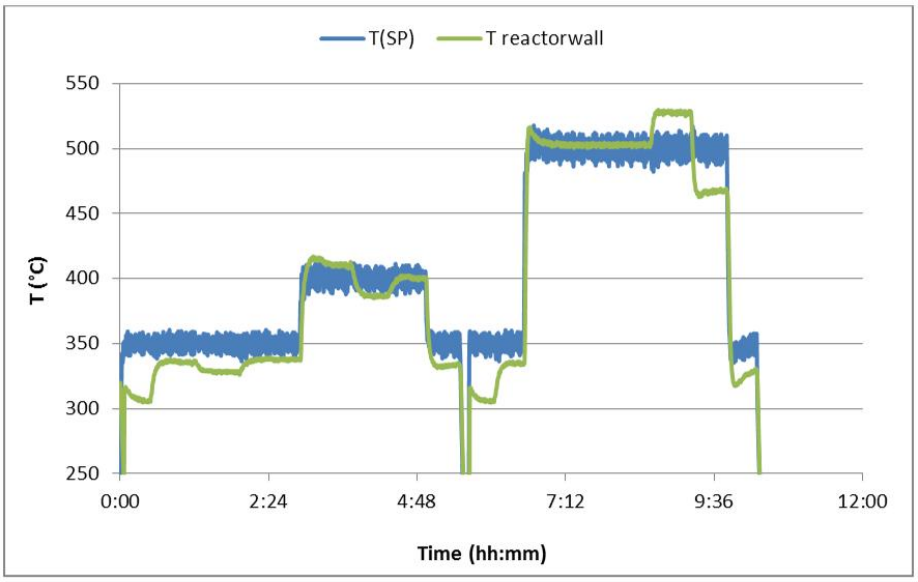

Figure 6.17: Temperature in the reactor wall and temperature set point vs. reaction time. Results from washcoated reactor with 20.6 mg of nickel content.

Figure 6.17 and Figure 6.18 show the variations of the temperature on the reactor wall due to set point variations (flow rate and/or temperature). The reactor where the washcoated catalyst was applied allowed efficient temperature control. The temperature on the reactor wall was close to the set point in every case with a maximum difference of 50^0C. The temperature was higher in the reactor due to the heat release from the exothermic methanation when the flow rate was increased. Conversely, the heat control in the packed-bed reactor was poor at low temperature set points (350 and 400^0C). At those conditions, inefficient heat removal possibly resulted in

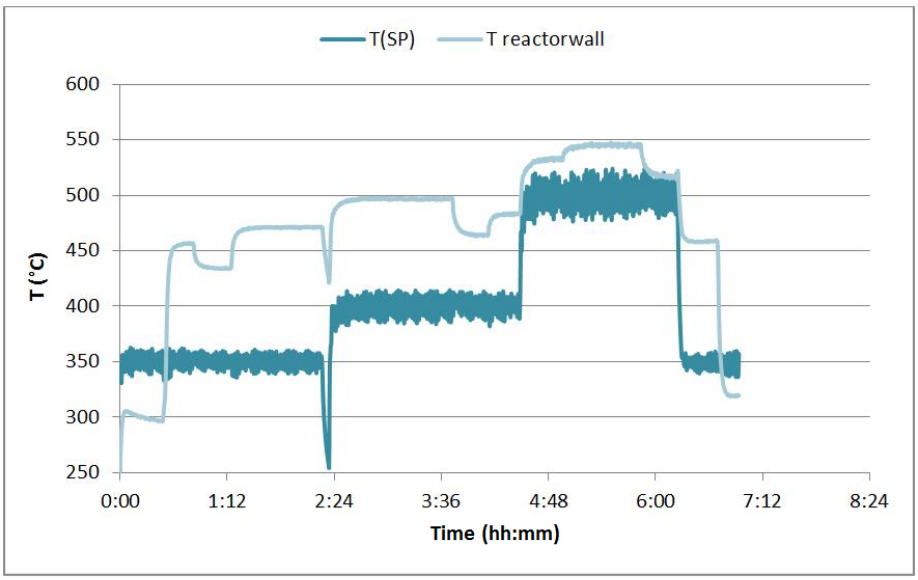

Figure 6.18: Temperature in the reactor wall and temperature set point vs. reaction time. Results from packed-bed reactor with 18.2 mg of nickel content.

hot-spot formation. The heat released by the exothermic methanation was not efficiently removed which increased the temperature in the catalyst bed.

Figure 6.19 shows the CO_2 conversion of methanation performed in washcoated and packed-bed reactors with 20.6 and 18.2 mg of nickel respectively. The clearest difference between the reactors was the range of reaction temperatures. Both reactors were operated with exactly the same flow rate (1.0 ln/min) and temperature set points (350, 400 and 500^{0}C). However, heat management features of each reactor led to different reactor wall temperature. Conversions were almost unaffected by variations on the reaction temperature in the packed-bed reactor. Therefore, methanation in this reactor can be assumed to be close to the equilibrium state in the entire operational range. In contrast, in the washcoated reactor methanation was close to the equilibrium state only at the highest temperature set value. The performance was improved at higher temperatures due to increased reaction rate passing from 10% of CO_2 conversion to 60%.

W_{Ni}HSV considers flow rate and nickel content of the catalysts. Figure 6.20 shows that variations in W_{Ni}HSV caused no change in the performance of the washcoated catalyst, and little change in the packed-bed catalyst. However, slightly more CO_2 was converted in the packed-bed reactor due to approximately 50 degrees higher operation temperature (Figure 6.19). Therefore, the catalyst loading technique did not imply evident difference in the CO_2 conversion.

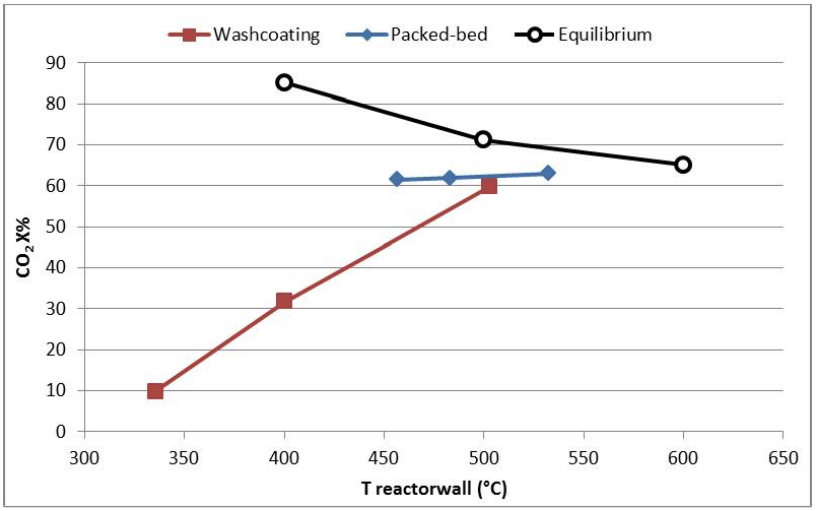

Figure 6.19: Effect of the reaction temperature on the CO_2 conversion in methanation on washcoated catalyst and packed-bed catalyst.

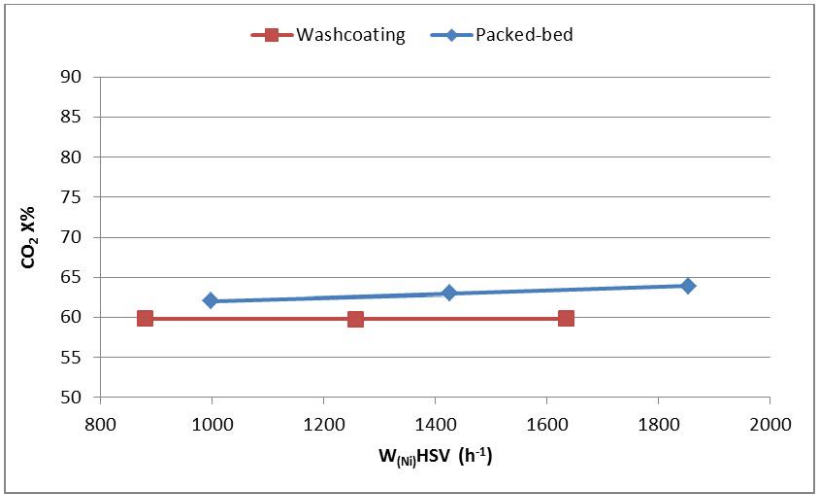

Figure 6.20: Effect of the $W_{Ni}HSV$ on the CO_2 conversion of methanation over washcoated and packed-bed catalysts at temperature set point equal to 500^0C.

Figure 6.21 shows methane selectivity close to 90% in the washcoated catalyst, and close to 50% in packed-bed reactor around 500^0C. The packed-bed reactor methanation achieved the chemical equilibrium in every set point. Therefore the selectivity followed the thermodynamics trend, the catalyst exhibited lower methane selectivity at higher temperatures. Conversely, methanation only reached the chemical equilibrium at the highest temper-

ature set point in the washcoated reactor. Thus, the reaction performance improved at higher temperature.

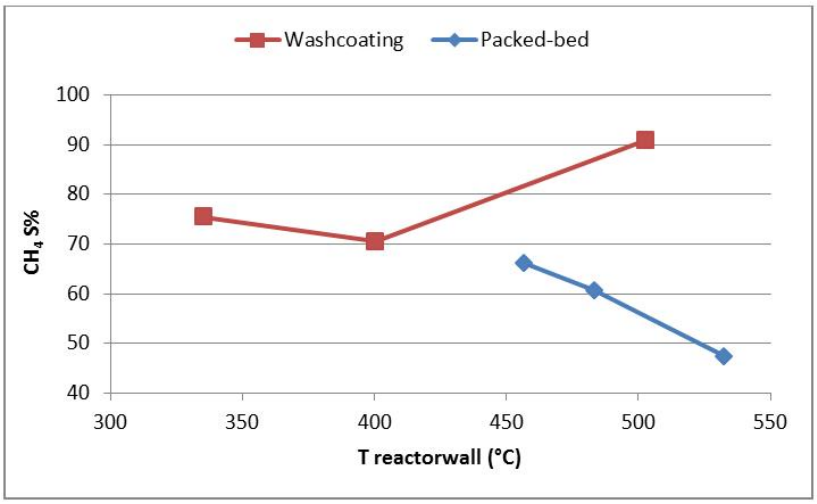

Figure 6.21: Effect of the reaction temperature on the CH_4 selectivity in methanation over washcoated catalyst and packed-bed catalyst.

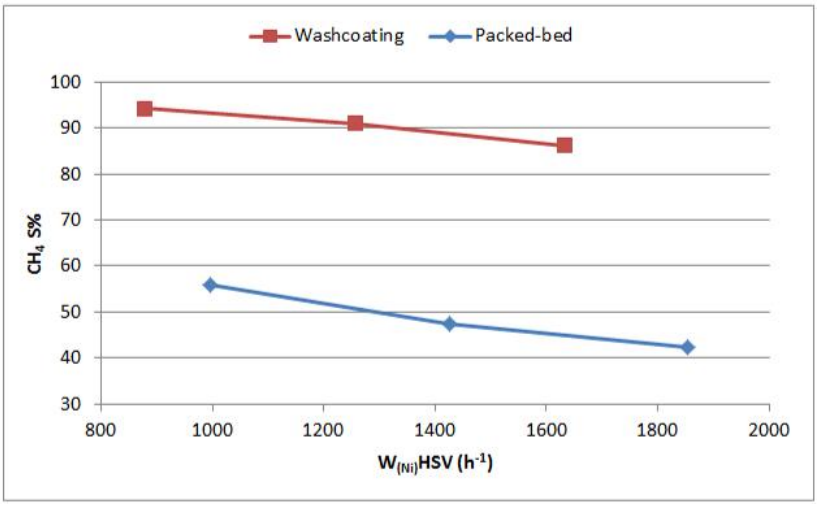

Figure 6.22: Effect of the $W_{Ni}HSV$ on the CH_4 selectivity in methanation over washcoated catalyst and packed-bed catalyst at temperature set point equal to 500^0C.

Considering the amount of nickel in the catalyst Figure 6.22 shows higher selectivity towards methane in washcoated reactor than in packed-bed reactor. Methane selectivity was significantly affected by the catalyst loading

technique. Washcoated catalyst obtained better selectivity towards methanation due to enhanced control of the temperature. Conversely, in the packed-bed reactor the rWSR was promoted because of heat removal deficiency.

Yield of methane follows similar tendency as selectivity for both catalyst. Also in this case the yield of methane was enhanced at higher temperatures in washcoated catalyst, while yield decreased in packed-bed reactor.

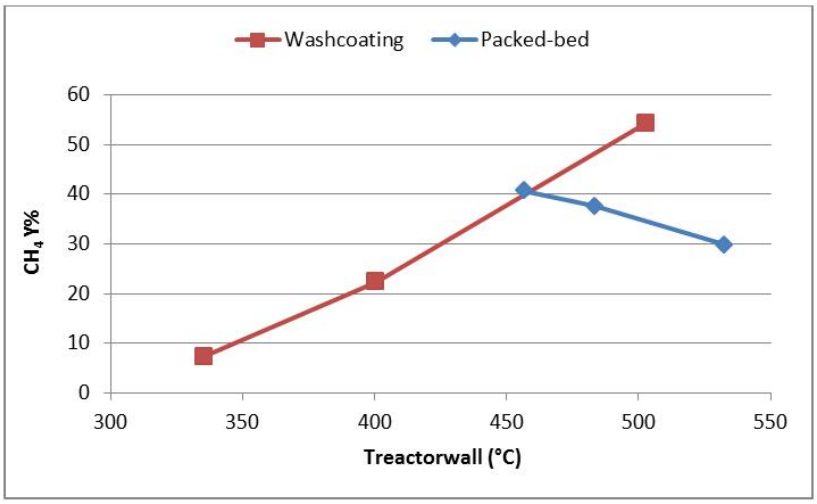

Figure 6.23: Effect of the reaction temperature on the CH_4 yield of methanation over washcoated catalyst and packed-bed catalyst.

Table 6.3 shows the performance of two different washcoated catalysts and a packed-bed catalyst. Comparing catalysts with similar nickel content, the performance of washcoated catalyst was superior to packed-bed catalyst at high temperature. Although the carbon dioxide conversion was slightly higher in packed-bed catalyst, lower selectivity towards methane resulted in lower CH_4 yield. In the washcoated reactor the CH_4 yield was approximately 15% higher than in the packed-bed reactor with similar amount of nickel.

The washcoat with the highest content of nickel (Table 6.3) exhibited good CO_2 conversion. Additionally, the methane selectivity reach excellent value (98%) that rose the yield up to 65%. Aziz *et al.* [15] obtained similar results, although with modestly higher methane selectivity. They performed several experiments in fixed-bed of nickel-based catalysts on different supports. In a comparable case to the results obtained with the 69.0 mg of nickel washcoat, they utilized mesostructured silica nanoparticles as support. However, the temperature conditions set in those experiments was milder (300^0C).

Reactor	T (^{0}C)	CO_2 X%	CH_4 S%	CO S%	CH_4 Y%
	336	9.8	75.4	24.6	7.4
20.6 WC	400	31.8	70.5	29.5	22.4
	503	59.8	90.8	9.2	54.3
	373	32.9	88.4	11.6	29.1
69.0 WC	430	55.9	94.1	5.9	52.6
	422	66.8	98.1	1.2	65.6
	457	61.6	66.2	33.8	40.7
18.2 PB	483	62.0	60.6	39.4	37.5
	532	63.0	47.4	52.6	29.8

Table 6.3: Reaction parameters of methanatio performed in washcoated reactors and in a packed-bed reactor. Results obtained at different temperatures and flow rate equal to 1 ln/min.

6.6 Nanocoated Catalyst

The third type of catalysts tested in this study were nanocoats. These catalysts had nickel contents in the order of 10^{-4} g. In contrast, the catalysts evaluated until now (packed-bed and washcoated catalysts) had nickel contents in the order of 10^{-2} g.

Flow rate of 1.3 ln/min provided short residence time the methanation performance was negligible. Accordingly, the flow rate was decreased to 0.3 ln/min to increase the residence time. Despite this adaptation, the conversion was considerably low. Therefore, a gas chromatograph was used to detect and measure the product outlet composition instead of the on-line analyser.

Figure 6.24 shows the conversion obtained with the reactor that contained the lowest amount of nickel at different temperatures. Other nanocoated catalysts with different concentrations exhibited similar trends. Conversion increased at higher temperatures and lower flow rate.

Figure 6.25 and Figure 6.26 respectively show carbon dioxide conversion and methane selectivity of methanation conducted in the nanocoated reactors with the lowest and the highest nickel content. Slightly higher temperatures on the reactor wall and improved performance of the nanocoated reactor with highest amount of nickel are the main observations. Furthermore, the CH_4 selectivity plotted for the catalyst with highest amount of nickel showed an inspected tendency. Methane selectivity increased when the temperature set point was risen from 350 to 400^{0}C. Conversely, the selectivity decreased when the variation was from 400 to 500^{0}C.

A blank reactor, and a reactor solely washcoated with the catalyst support were also tested. The objective was to study the extent uncatalysed reactions, and the activity of the catalyst support for the methanation of

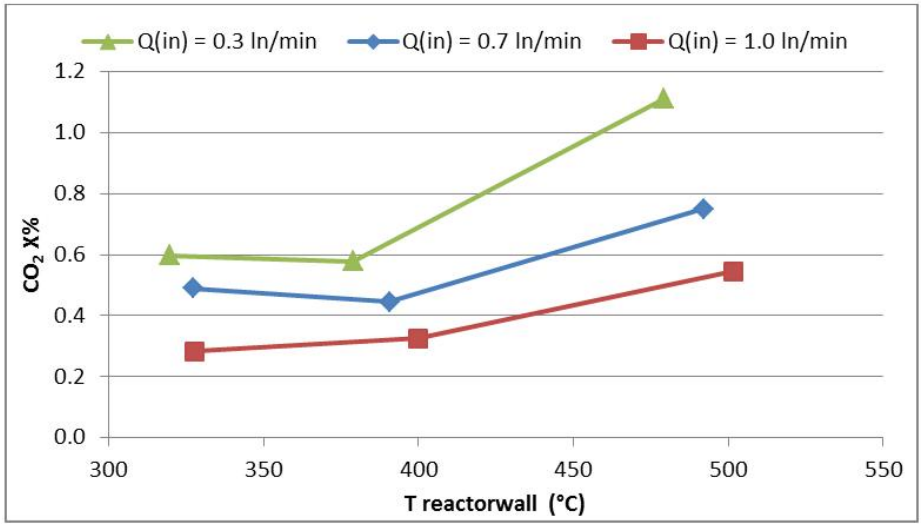

Figure 6.24: Effect of the reaction temperature on the CO_2 conversion in methanation at different flow rates. Results from reactor nanocoated with the lowest nickel-content catalyst.

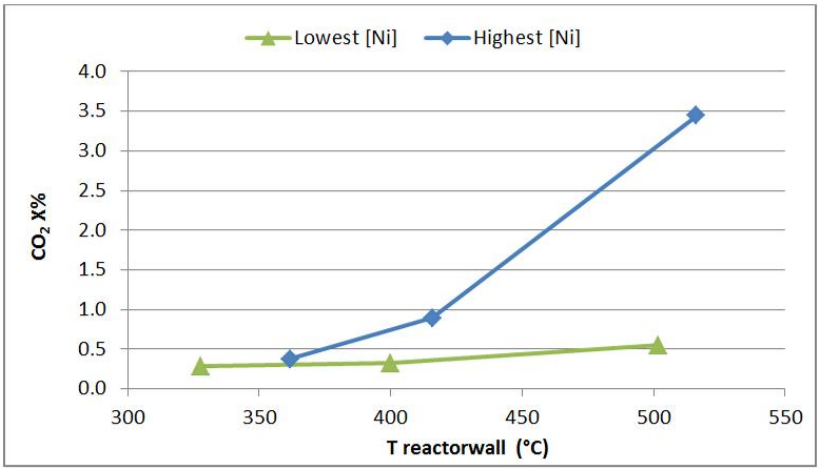

Figure 6.25: Effect of the reaction temperature at inlet flow rate of 1 ln/min on the CO_2 conversion of methanation for different amounts of nickel content in the catalyst. Results from reactor nanocoated with the lowest and highest nickel-content catalyst.

carbon dioxide. The comparison of results from those experiments with the results obtained with nanocaoted catalysts also enabled to assess the catalytic activity of the nanocoats.

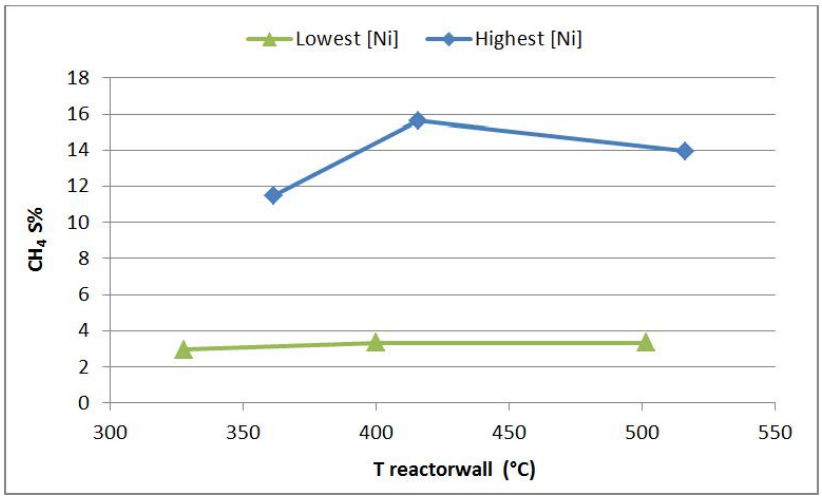

Figure 6.26: Effect of the reaction temperature at inlet flow rate of 1 ln/min on the CH_4 selectivity of methanation for different amounts of Ni content in the catalyst. Results from reactor nanocoated with the lowest and highest nickel-content catalyst.

Reactor	T (^{0}C)	CO_2 X%	CH_4 S%	CO S%	CH_4 Y%
	401	0.4	3.2	96.8	0.01
Blank	453	0.4	4.1	95.9	0.02
	536	0.8	0.8	99.2	0.01
	344	0.6	5.4	94.6	0.03
Support	394	1.7	12.8	87.2	0.21
	486	7.4	10.3	89.7	0.76
	328	0.3	3.0	97.0	0.01
L	400	0.3	3.4	96.6	0.01
	502	0.5	3.3	96.6	0.02
	363	0.4	13.9	86.1	0.05
SL	414	0.9	29.8	70.2	0.26
	335	0.2	9.2	90.8	0.02
SH	380	0.2	3.7	96.3	0.01
	469	0.3	5.1	94.9	0.01
	362	0.4	11.5	88.5	0.04
H	416	0.9	15.6	84.4	0.14
	516	3.4	14.0	86.0	0.48

Table 6.4: Reaction parameters of methanation performed in a blank reactor, wash-coated reactor with the catalyst support, and nanocoated reactors with different nickel contents. Results obtained at different temperatures and flow rate equal to 1 ln/min. The amount of nickel in the reactor: highest (H), second highest (SH), second lowest (SL), and lowest (L).

Table 6.4 shows higher conversions in the blank reactor than in any of the nanocoated reactors, except the one with the highest nickel content. Low conversion and low CH_4 selectivity resulted in almost zero yields of methane

in the nanocoated catalysts. The catalyst support also achieved higher CO_2 conversion and CH_4 selectivity than any of the nanocoats. Therefore, the nanocoated catalyst did not accomplish catalytic performance required for methanation. Furthermore, it can be assumed that the reactions occurred in the blank reactor were thermally originated. In contrast, catalytic reactions occurred in the reactor washcoated with catalyst support. However the catalytic activity was not comparable to the washcoated or packed-bed catalysts.

Chapter 7

Error Sources

This section evaluates the most significant error sources found during the execution of this experimental work. The analysis of error sources will provide justification for some of the results discussed in Section 6.

The experimental set up, and analysis and measurements methods, are the main error sources that will be discussed in this chapter. The first section is focused on the set up, specifically the reactors and the heat suppliers. Analysis methods and flow meter and thermocouple measurements will be considered in the second section.

7.1 Experimental set up

The heating elements which supplied heat to the reactors were the principal error source of the experimental set up. Five different heating elements of the same type were attached to the reactors in straight contact with the back part of these. Therefore, differences in the attachment of the heating elements or the thermocouples which control those resulted in heterogeneous heat supply. In other words, the temperature of the reactor walls were different at the same temperature set point.

In set ups I and II, the heating element and the reactor were slightly separated in the area close to the reactor inlet. The thermocouple which controlled the heat supply was placed between the reactor and the heat element. This arrangement was problematic in terms of temperature control and homogeneity. First, the controlling thermocouple was in contact not only with the heating element, but also with the reactor wall. Thus, the control of the temperature in heating element was influenced by the temperature on the reactor wall. Second, the complexity involving the attachment of ther-

mocouples and heating elements to the reactors resulted in displacement of the thermocouples. (Figure 7.1) shows highlighted in red the tip of a thermocouple that should have been in contact with the heating element. The reactors where thermocouple displacements occurred were operated at higher temperatures. The tip of the misplaced thermocouples read lower surrounding temperature which resulted in reactors heated over the temperature set point.

Figure 7.1: Thermocouple displacement.

In order to overcome this error source, the controlling thermocouples were located in straight contact with the back part of the heating elements in set ups III, IV and V. However, the temperature distribution along the reactor was not noticeably improved. A possible explanation is the location of the controlling thermocouple. The thermocouple was attached in contact to the top of the heating element. Thus, that area was maintained at or close to the temperature set point. In contrast, lower parts of the heating element were not accurately controlled. Furthermore, poor insulation of the heating-element tail resulted in considerable heat losses. Consequently, lower parts of the reactor were at much lower temperature.

7.2 Analysis and measurement methods

On-line and gas chromatograph analysed the composition of outlet gas. The on-line analyser was calibrated approximately every two weeks to reduce analysis errors. However, this equipment was not considered as accurate as

gas chromatograph. On the other hand, the analysis of samples performed with gas chromatograph required a precise methodology to take advance of the accuracy. Therefore, measurement errors might be derived from the analysers and consequently reflected in the results.

The gas flow meter used to measure the product dry gas was considered accurate at higher flow rates than the outlet flow rate reached in these experiments. For this reason, the reaction mass balances were calculated using the composition data provided by the analyser and the mass carbon balance, as it was specified in Section 5.4.

Temperature is the reaction variable with the most significant effect on the reaction parameters of methanation. Thus, the major part of the results has been presented and evaluated in relation with the temperature. The thermocouples that measured the reaction temperature were located on the outer wall of the reactors. Consequently, the temperature in the core of the reaction was unknown. This represented a significant barrier of the experimental set up that limited a precise assessment of the results.

The temperature was measured on the reactor wall either at one point close to the mid-section of the reactor, or in several points along the length of few reactor. The temperature at the mid-section of the reactor was used to evaluate the performance of the reactor as the temperature of the whole system. Consequently, the comparability of different reaction system, such as packed-bed and washcoated catalyst, was difficult.

Several tests were conducted in reactors with similar amounts of catalyst in the set up IV in order to verify the repeatability of the experiments. Temperature was the main difference between reactors. In other words, the temperature measured on the reactor wall was different in each of the reactors at same temperature set points. Nevertheless, regarding catalyst performance the results were repeatable.

Chapter 8

Conclusions

Carbon dioxide methanation is a highly exothermic reaction. Therefore, the production of methane is favoured at low temperatures. However, methanation typically suffers from slow reaction rates at those temperatures. Novel catalysts applied in intensified reactors was proposed in order to meet the compromise between thermodynamics and kinetics, and thus, improve the reaction performance.

Control and management of heat supply to the reactors through the heating elements and by the exothermic reaction itself was challenging. Washcoated, intensified reactors showed improved ability for heat removal and more evenly distributed temperature than conventional packed-bed reactors. In the latter type of reactors, the temperature variations along the reactor length were minimized with the blocks-and-fins design which considerably enhanced the heat transfer and removal.

Packed-bed catalysts achieved approximately 60% CO_2 conversion close to the equilibrium state. This value is lower than the conversion reached in some of the works surveyed due to heat removal barriers found in the reactors. Selectivity towards methane was reported in literature ranging 90-100% in agreement with the thermodynamics. However, the maximum CH_4 selectivity obtained in the packed-bed reactors was close to 80%, and lower at higher operation temperatures. Heat transfer limitations in the packed-bed reactors resulted in hot spot formation that promoted the rWGS reaction. Consequently, the selectivity towards carbon monoxide increased affecting negatively the CH_4 yield.

Carbon dioxide methanation exhibited the best performance with washcoated catalysts at higher temperatures and low flow rate. The CO_2 conversions reached values around 60% at temperatures between 400 and 600^0C depending on the nickel content of the catalyst. The washcoats with lower nickel content required higher temperatures to achieve this conversion close

to the equilibrium state. The CH_4 selectivity at the same state maintained good values ranging from 84 to 99% in catalysts with nickel contents between 15 and 65 mg. However, the washcoat with 5 mg of nickel presented CH_4 selectivity under 50% at similar operating conditions. Thus, the performance of washcoated reactors improved in catalysts with higher nickel content. The reactor with highest amount of nickel (69 mg) reached 69% CO_2 conversion and 99% CH_4 selectivity at 410^0C. Furthermore, a washcoated catalyst with higher nickel loading but lower nickel content (34 mg) achieved similar values of conversion and selectivity. Therefore, it can be concluded that the activity of nickel-based catalysts was improved increasing the nickel loading.

GHSV was the most highlighted difference between packed-bed and washcoated reactors. Packed-bed reactors operated within the GHSV range of 20000 to 45000 1/h. In contrast, washcoated reactors worked at GHSV between 1000 and 2000 1/h. The catalyst bulk density of washcoated reactors was considerably lower than in packed-bed reactors. As a result, washcoated reactors presented more efficient management of the temperature. Additionally, the selectivity and yield of methane was higher in washcoated reactors. On the other hand, packed-bed showed deficient control of the temperature. Therefore, methane selectivity was lower than with the majority of the washcoated catalysts, or than with nickel packed-bed considered in the literature.

The tests conducted with nanocoated catalysts were unsuccessful. Carbon dioxide conversion was considerably low compared to washcoated or packed-bed catalysts. Indeed, the results obtained with the blank reactor and with the nanocoated reactors presented almost no difference. Only the nanocoat with the highest nickel content exhibited some activity.

Chapter 9

Recommendations for further studies

Improvements can be included in the experimental set up in order to enhance the temperature management in the reactors. Already in this work the blocks-and-fins structure facilitated the heat removal and even the temperature along the reactor. In addition, better insulation of the reactors and surrounding areas, and changes in the location of the controlling thermocouples are recommended for a more homogeneous distribution of the temperature.

The washcoated catalyst with higher percentage of nickel loading exhibited better performance than other catalysts with higher mass of nickel. The reduction of overall nickel content could reduce the catalyst costs. However, the only case assessed in this work involved noticeable decrease of CH_4 selectivity (6.70%) during the stabilization period of the catalyst. Therefore, further research work should be done with this type of catalyst in order to prove the benefits of higher nickel loadings. Furthermore, the tests carried out with washcoated catalysts resulted in good performance in general. Thus, research activities could be focussed on the development of scaled-up washcoated reactors.

Nanocoated catalysts show better metal dispersion than other catalysts deposited with different techniques. Accordingly, the possibility of reducing nickel loading needs could significantly reduce catalyst costs. The performance of these catalysts may be enhanced using more active metals, or active combinations of these, deposited on suitable carriers. This motivates further research on nanocoating technology in order to develop catalysts with significantly lower content of active phase.

Bibliography

[1] International Energy Agency (IEA). 2014; `http://www.iea.org/`.

[2] D.Y.C. Leung, M. M.-V., G. Carmanna *Renewable and Sustainable Energie Reviews* **2014**, *39*, 426–443.

[3] Herzog, H. *Energy Economics* **2011**, *33*, 597–604.

[4] J. Koornneef, C. H. C. H.-M. H. K. K. M. K. T. D. A. C., P. van Breevoort *International Journal of Greenhouse Gas Control* **2012**, *11*, 117–132.

[5] Wee, J.-H. *Applied Energy* **2013**, *106*, 143–151.

[6] Y. Sanchez-Vicente, M. P. J. K.-M. G., T.C. Drage *International Journal of Greenhouse Gas Control* **2013**, *13*, 78–86.

[7] Ganesh, I. *Renewable and Sustainable Energie Reviews* **2014**, *31*, 221–257.

[8] R.-J. Wei, B.-Y. D.-Z.-Q. F. G.-R. Q., X.-H. Zhang *Journal of Molecular Catalysis A: Chemical* **2013**, *379*, 38–45.

[9] C.A. Stewart, B. M. R. K., D.A. Dickie *Polyhedron* **2012**, *32*, 14–23.

[10] M. Specht, F. B. B. F. V. F.-B. S. M. S. G. W., U. Zuberbühler *FVEE. AEE Topics* **2009**, 69–78.

[11] Ch. Breyer, M. S. J. S., S. Rieke Hybrid PV-wind-renewable methane power plants - A potential cornerstone of global energy supply. 2011.

[12] Sterner, M. Bioenergy and renewable power methane in integrated 100% renewable energy systems. Limiting global warming by transforming enrgy systems. Ph.D. thesis, Faculty of Electrical Engineergina and Computer Sciende of University of Kassel, Germany, 2009.

[13] M. Götz, D. B. S. B., R. Reimert Storage of volatile renewable energy in the gas grid applying 3-phase methanation. 2011.

[14] W. Wang, J. G. *Front. Chem. Sci. Eng.* **2011**, *5(1)*, 2–10.

[15] M.A.A. Aziz, S. T. R. M. Y. T.-Y. M. S., A.A. Jalil *Applied Catalysis B: Environmental* **2014**, *147*, 359–368.

[16] S. Tada, R. K. T. H. H. K., O.J. Ochieng *International Journal of Hydrogen Energy* **2014**, *39*, 10090–10100.

[17] S. Rahmani, F. M., M. Rezaei *Journal of Industrial Engineering Chemistry* **2014**, *20*, 1346–1352.

[18] A.H. Zamani, W. B., R. Ali *Journal of the Taiwan Institute of Chemical Engineers* **2014**, *45*, 143–152.

[19] C. Swalus, C. P. P. B. P. R., M. Jacquemin *Applied Catalysis B: Environmental* **2012**, *125*, 41–50.

[20] A. Beuls, M. J. G. H. A. K.-P. R., C. Swalus *Applied Catalysis B: Environmental* **2012**, *113-114*, 2–10.

[21] T. Yoshida, Y. T. T. H. T. H.-K. O., M. Tsuji *Energy Convers. Mgmt* **1997**, *38*, S443–S448.

[22] K.P.Brooks, H. Z. R. J. K., J. Hu *Chemical Engineering Science* **2007**, *62*, 1161–1170.

[23] Y. Men, R. Z. V. H. H. L., Gu. Kolb *Catalysis Today* **2007**, *125*, 81–87.

[24] M. Miyamoto, Y. M. Y. O. S. U.-M. A., R. Hayakawa *International Journal of Hydrogen Energy* **2014**, *39*, 10154–10160.

[25] D. Schlereth, O. H. *Chemical Engineering Research and Design* **2014**, *92*, 702–712.

[26] H. Ohya, H. K. K. I. H. O.-M. A. S. T. Y. N., J. Fun *Journal of Membrane Science* **1997**, *131*, 237–247.

[27] G. Kolb, V. H. *Chemical Engineering Journal* **2004**, *98*, 1–38.

[28] R. Guettel, T. T. *Chemical Engineering Science* **2009**, *64*, 955–964.

[29] M.J. Economides, D. W. *Journal of Natural Gas Science and Engineerging* **2009**, *1*, 1–13.

[30] K. Aasberg-Petersen, C. O. N. S. J. S. S. T., I. Dybkjaer *Journal of Natural Gas Science and Engineerging* **2011**, *3*, 423–459.

[31] S. Walspurger, J. D. M. S. W. H., G.D. Elzinga *Chemical Engineering Journal* **2014**, *242*, 379–386.

[32] Comision, E. Quarterly Report on European Gas Markets. 2013.

[33] K. Müller, F. R., M. Fleige; SchmeiBer, D. *Energy Procedia* **2013**, *40*, 240–248.

[34] S. Strauch, O. J., T. Schulzke Alternative ways of biomethane production. 2014.

[35] J.-N. Park, E. M. *Journal of Catalysis* **2009**, *266*, 92–97.

[36] J. Gao, Y. P. D. H. G. X. F. G. F. S., Y. Wang *RSC Advances* **2012**, *2*, 2358–2368.

[37] W. Zhen, G. L. J. M., B. Li *RSC Advances* **2014**, *4*, 16472–16479.

[38] S. Takenaka, K. O., T. Shimizu *International Journal of Hydrogen Energy* **2004**, *29*, 1065–1073.

[39] G. Jing, F. W.-P. L. Q.-B. S. H., J. Li-Shan *J Fuel Chem Technol* **2009**, *37(5)*, 573–577.

[40] M. Lehner, H. S. M. K., R. Tichler In *Power-to-Gas: Tehcnology and Business Models*; in Energy, S. B., Ed.; Springer, 2014.

[41] S. VErma, N. C. T. R., C.S. Oakes *Energy Procedia* **2011**, *4*, 2340–2347.

[42] F. Ocampo, A.-C. R., B. Louis *Applied Catalysis A: General* **2009**, *369*, 90–96.

[43] F. Ocampo, L. K.-M. A.-C. R., B. Louis *Applied Catalysis A: General* **2011**, *392*, 36–44.

[44] H. Song, J. Z.-L. C., J. Yang *Chinese Journal of Catalysis* **2010**, *31*, 21–23.

[45] C. Galletti, V. S., S. Specchia *Chemical Engineering Journal* **2011**, *167*, 616–621.

[46] E. Jwa, H. L.-Y. M., S.B. Lee *Fuel Processing Technology* **2013**, *108*, 89–93.

[47] P. Dinka, A. M. *Journal of Power Sources* **2007**, *167*, 472–481.

[48] D. Fu, M. I. In *Ferroelectrics - Material Aspects*; Lallart, M., Ed.; CC BY-NC-SA, 2011; Vol. Chapter 20.

[49] T. Salmi, J., J.-P. Mikkola In *Chemical Reaction Engineering and Reactor Technology. A Series of Refernce Books and Textbooks*, chemical industries ed.; Hinemann, H., Ed.; Taylor & Francis Group: New York, 2011; Vol. 125.

[50] W. de Vries, M. o. E. A. *Creative Energy. Energy Transition.*

[51] E. Tronconi, C. V., G. Groppi *Current Opinion in Chemical Engineering* **2014**, *5*, 55–67.

[52] ETOGAS. `http://www.etogas.com/`.

[53] Y.-L. Kao, Y.-T. T. I.-L. C. J. W., P.-H. Lee *Journal of Taiwan Institute of Chemical Engineers* **2014**, *xxx*, xxx–xxx.

[54] S. Bajhr, M. G. Development of a methanation process for PtG appliances. 2013.

[55] Z. Anxionnaz, C. G. P. T., M. Cabassub *Chemical Engineering and Processing* **2008**, *47*, 2029–2050.

[56] A. Gavriilidis, E. C. K. Y., P. Angeli; Wan, Y. *Trans IChemE* **2002**, *80*.

[57] K. Kusakabe, A. G. V. H. H. O. K.-I. S. P. W. J.-i. Y., J.G.E (Han) Gardeniers *Chemical Engineering Journal* **2011**,

[58] L. Kiwi-Minsker, A. R. *Catalysis Today* **2005**, *110*, 2–14.

[59] O. Görke, K. S., P. Pfeifer *Applied Catalysis A: General* **2009**, *360*, 232–241.

[60] P.L. Mills, J. R., D.J. Quiram *Chemical Engineering and Science* **2007**, *62*, 6992–7010.

[61] M.Zanfir, A. G. *Chemical Engineering Science* **2003**, *58*, 3947–3960.

[62] A.Y. Tonkovich, Y. W. D. Q. T. L. W. R., S. Perry *Chemical Engineering Science* **2004**, *59*, 4819–4824.

[63] Velocys. 2013; `http://www.velocys.com/`.

[64] T. Lange, C. L. H. H. E. K., S. Heinrich *Chemical Engineering Science* **2012**, *69*, 440–448.

[65] Pfeifer, P. In *Application of catalysts to metal microreactor systems, Chemical Kinetics*; Patel, D. V., Ed.; InTech, 2012.

[66] J. Knochen, C. K. T. T., R. Güttel *Chemical Engineering and Processing* **2010**, *49*, 958–964.

[67] O. Görke, K. S., P. Pfeifer *Catalysis Today* **2005**, *11*, 132–139.

[68] R.E. Hayes, J. M., A. Rojas *Catalysis Today* **2009**, *147S*, S113–S119.

[69] M. Saber, C. P.-H. D. E., T.T. Huu *Chemical Engineering Journal* **2012**, *185-186*, 294–299.

[70] E. Bianchi, C. V.-G. G. H. F. E. T., T. Heidig *Chemical Engineering Journal* **2012**, *198-199*, 512–528.

[71] J. von Rickenbach, C. N. P. E. D. P., F. Lucci *International Journal of Heat and Mass Transfer* **2014**, *75*, 337–346.

[72] E. Bianchi, C. V. G. G. H. F. E. T., T. Heidig *Catalysis Today* **2013**, *216*, 121–134.

[73] Y. Liu, L. N. D. B. P. N. C. P.-C. P.-H., D. Edouard *Chemical Engineering Journal* **2013**, *222*, 265–273.

[74] M. Sheng, D. C. B. T., H. Yang *Journal of Catalysis* **2011**, *281*, 254–262.

[75] W. Chen, F. C. Y. L., W. Sheng *International Journal of Hydrogen Energy* **2012**, *37*, 18021–18030.

[76] M. Sheng, H. Y. C. G. W. Y. J. D. H. B. T., D.R. Cahela *International Journal of Heat and Mass Transfer* **2013**, *56*, 10–19.

[77] M. Sheng, D. C. W. Y. J. C. G. B. T., H. Yang *Applied Catalysis A: General* **2012**, *445-446*, 143–152.

[78] V.M. Lebabier, L. K. A. X. L. L. L. C. T. X. B. Y. W., R.A. Dagle *Applied Catalysis B: Environmental* **2014**, *144*, 223–232.

[79] X. Hu, W. D. J. Y. Y. H., W. Yan *Chinese Journal of Catalysis* **2013**, *34*, 1720–1729.

[80] S. Smart, J. S. A. B. J. D. d. C., S. Liu *Woodhead Publishing Limited* **2014**, 182–217.

[81] A. Zhen, J. F. T. C., F. Jones *AIChE Journal* **2000**, 284.

[82] T. Cui, J. M. J. G. R. B. B. E., J. Fang *AIChE Journal* **2000**, 488.

[83] N. Di Miceli Raimondi, N. G. M. C. C. G., N. Olivier-Maget *Chemical Engineering Research and Design* **2014**, *xxx*, xxx–xxx.

[84] X. Guo, L. L., Y. Fan *Energy* **2014**, *69*, 728–741.

[85] F. Théron, M. C. C. G. P. T., Z. Anxionnaz-Minvielle *Chemical Engineering and Processing* **2014**, *82*, 30–41.

[86] J. C. Park, D. C. H. J. J.-I. Y., N.S. Roh *Fuel Processing Technology* **2014**, *119*, 60–66.

[87] L. Despènes, C. G. M. C., S. Elgue *Chemical Engineering and Processing* **2012**, *52*, 102–111.

[88] M. Mbodji, L. F. D. D. M. F. R.-L. P. S. V. R. J. P. D.-G., J.M.Commenge *Chemical Engineering Journal* **2012**, *207-208*, 871–884.

[89] SULZER. `http://www.sulzer.com/`.

[90] HEATRIC. Printed Circuit Heat Exchangers. 2015; `http://www.heatric.com/`.

[91] J. Gao, J. L. M. Z. F. G.-G. X. Z. Z. F. S., C. Jia *Journal of Energy Chemistry* **2013**, *22*, 919–927.

[92] F.W. Chang, M.-T. T. M.-C. H., M.-S. Kuo *Applied Catalysis A: General* **2003**, *247*, 309–320.

[93] G. Garbarino, L. M.-G. B., P. Riani *International Journal of Hydrogen Energy* **2014**, *39*, 11557–11565.

[94] Kolb, G. *Chemical Engineering and Processing* **2013**, *65*, 1–44.

[95] ABB, 2014; `http://www.abb.com/`.

Appendices

Appendix A

Experimental set up

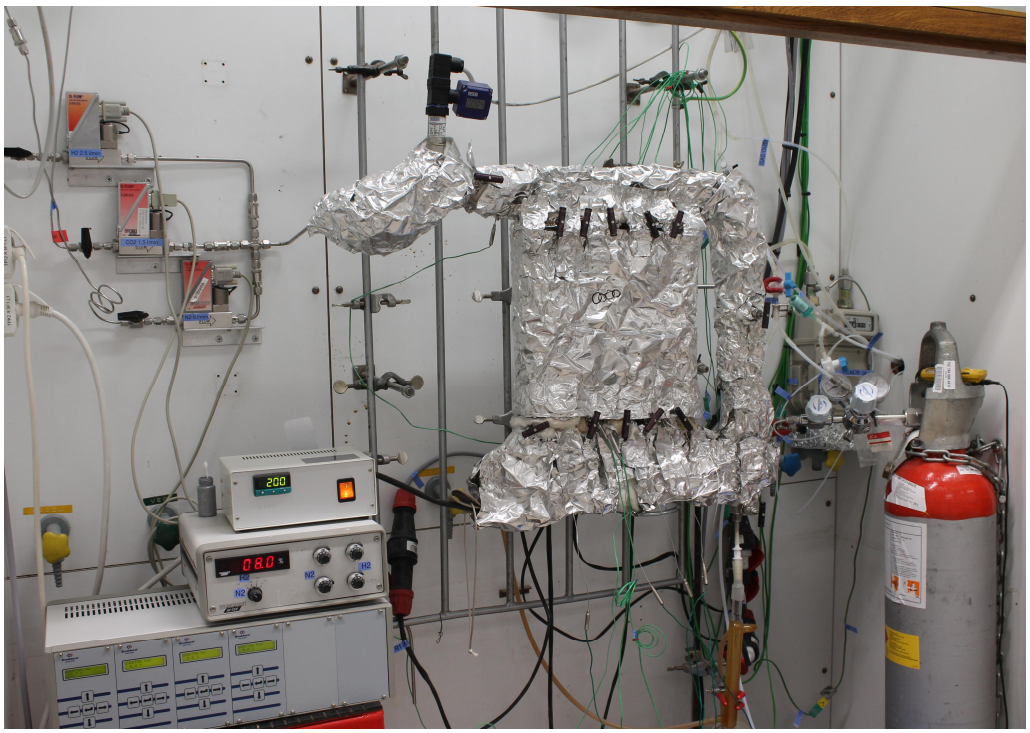

Figure A.1: Picture of the equipment and accessories used for carbon dioxide methanation.

Appendix B

List of Experiments and Catalysts

SU	Set Point		Reactor				
	T (^{0}C)	Q^{in} (ln/min)	1	2	3	4	5
I	350	0.7	43.01 WC	20.57 WC	64.43 WC	69.02 WC	45.73 WC
		1.0	43.01 WC	20.57 WC	64.43 WC	69.02 WC	45.73 WC
		1.3	43.01 WC	20.57 WC	64.43 WC	69.02 WC	45.73 WC
		2.0	43.01 WC				45.73 WC
	400	0.7	43.01 WC	20.57 WC	64.43 WC	69.02 WC	45.73 WC
		1.0	43.01 WC	20.57 WC	64.43 WC	69.02 WC	45.73 WC
		1.3	43.01 WC	20.57 WC	64.43 WC	69.02 WC	45.73 WC
		2.0	43.01 WC				45.73 WC
	450	1.0			64.43 WC		
	500	0.7	43.01 WC	20.57 WC	64.43 WC	69.02 WC	45.73 WC
		1.0	43.01 WC	20.57 WC	64.43 WC	69.02 WC	45.73 WC
		1.3	43.01 WC	20.57 WC	64.43 WC	69.02 WC	45.73 WC
		2.0	43.01 WC				45.73 WC
	550	1.0			64.43 WC		

Table B.1: List of the experiments performed during the experimental research, and type of catalyst and the amount of nickel in the catalyst. Types of catalyst: Packed-bed (PB), Washcoat (WC), Nanocoat (NC), and catalyst support (CS). The amount of nickel is expressed by: mass of nickel in mg (numbers), highest (H), second highest (SH), second lowest (SL), and lowest (L).

SU	Set Point		Reactor				
	T (^{0}C)	Q^{in} (ln/min)	1	2	3	4	5
II	350	0.3	SL NC	SL NC	L NC		
		0.7	SL NC	SL NC	L NC	5.27 WC	
		1.0	SL NC		L NC	5.27 WC	Blank
		1.3				5.27 WC	
	400	0.3	SL NC		L NC		
		0.7	SL NC		L NC	5.27 WC	
		1.0	SL NC	SL NC	L NC	5.27 WC	Blank
		1.3				5.27 WC	
	500	0.3	SL NC		L NC		
		0.7	SL NC		L NC	5.27 WC	
		1.0		SL NC	L NC	5.27 WC	Blank
		1.3				5.27 WC	
III	350	0.7		33.80 WC	18.15 PB		
		1.0	CS	33.80 WC	18.15 PB	H NC	SH NC
		1.3		33.80 WC	18.15 PB		
	400	0.7		33.80 WC	18.15 PB		
		1.0	CS	33.80 WC	18.15 PB	H NC	SH NC
		1.3		33.80 WC	18.15 PB		
	500	0.7		33.80 WC	18.15 PB		
		1.0	CS	33.80 WC	18.15 PB	H NC	SH NC
		1.3		33.80 WC	18.15 PB		
IV	350	0.7	15.30 WC	16.80 WC	15.00 WC	16.00 WC	
		1.0	15.30 WC	16.80 WC	15.00 WC	16.00 WC	
		1.3	15.30 WC	16.80 WC	15.00 WC	16.00 WC	
	400	0.7	15.30 WC	16.80 WC	15.00 WC	16.00 WC	
		1.0	15.30 WC	16.80 WC	15.00 WC	16.00 WC	
		1.3	15.30 WC	16.80 WC	15.00 WC	16.00 WC	
	500	0.7	15.30 WC	16.80 WC	15.00 WC	16.00 WC	
		1.0	15.30 WC	16.80 WC	15.00 WC	16.00 WC	
		1.3	15.30 WC	16.80 WC	15.00 WC	16.00 WC	
V	350	0.7		15.30 PB			
		1.0		15.30 PB			15.45 PB
		1.3		15.30 PB			
		2.0		15.30 PB			
	400	1.0					15.45 PB
		0.7					15.45 PB
	500	1.0					15.45 PB
		2.0					15.45 PB

Table B.2: Continuation Table B.1. List of the experiments performed during the experimental research, and type of catalyst and the amount of nickel in the catalyst. Types of catalyst: Packed-bed (PB), Washcoat (WC), Nanocoat (NC), and catalyst support (CS). The amount of nickel is expressed by: mass of nickel in mg (numbers), highest (H), second highest (SH), second lowest (SL), and lowest (L).

Appendix C

Analysis Methods

Analyser Module	Name	Sample Gas	Measurement Range (vol-%)
Thermal conductivity	Caldos 25	H_2 in N_2	0-100
Thermomagnetic	Magnos 27	O_2	0-25
Infrared photometer	Uras 26	CO_2, CO and CH_4	0-50 , 0-50 and 0-30

Table C.1: Online analyzer modules and features. Adapted from [95].

Gas	Component	Composition (vol-%)
Scan 1	CO_2	15.00
	CO	15.00
	CH_4	3.03
	N_2	66.97
Scan 2	H_2	15.00
	N_2	85.00

Table C.2: Online analyzer calibration gases composition.

Component	Composition
H_2	12.50 vol-%
CO_2	9.93 vol-%
CO	18.00 vol-%
CH_4	4989 ppm
C_2H_6	4985 ppm
C_2H_4	5012 ppm
C_2H_2	4861 ppm
N_2	57.60 vol-%

Table C.3: Gas chromatograph calibration gas composition.